PHILOSOPHICAL TRANSACTIONS OF THE ROYAL SOCIETY B BIOLOGICAL SCIENCES

Biology and Physics of Locust Flight. III. The Aerodynamics of Locust Flight

Martin Jensen

Phil. Trans. R. Soc. Lond. B 1956 **239**, 511-552
doi: 10.1098/rstb.1956.0009

BIOLOGY AND PHYSICS OF LOCUST FLIGHT
III. THE AERODYNAMICS OF LOCUST FLIGHT

By MARTIN JENSEN*
Professor August Krogh's Laboratory, Søbredden 24, Gentofte, Denmark

(*Communicated by J. W. S. Pringle, F.R.S.—Received 16 July 1955*)

CONTENTS

* Now at Vindlaboratoriet, Danmarks tekniske Højskole, Copenhagen.

A proper understanding of how locusts fly must be based upon knowledge of how the wings are moved. A desert locust was suspended from a balance and placed in an air stream so that it flew under nearly the same conditions as during natural forward flight. Four stroboscopic slow-motion films were selected for measurement. The movements of the wings, i.e. their positions, velocities and accelerations, were then calculated in sufficient detail to show how these quantities vary with time during one complete wing stroke.

The aerodynamic lift and drag of the entire natural wing were measured in a wind tunnel with the wing arranged in different positions relative to the flow. By placing it in the boundary layer of the tunnel, the wind speed was graded from tip to base in approximately the same way as during the actual flight. There is therefore no error due to scale effect or to the induced drag. In most respects the wings resemble ordinary, slightly cambered airfoils. Their characteristics are given as polar diagrams.

The kinematic and aerodynamic analyses make it possible to calculate the forces which act upon the locust at any instant of time. It is here necessary to presuppose that the non-stationary flight situations are essentially similar to a sequence of stationary situations. For locusts, this presupposition is justified: (i) from theoretical estimates of the quantitative effect of non-stationary flow; and (ii) from control measurements of the average thrust and lift produced during flight. It was found that the *calculated* vertical force, when averaged over an entire wing stroke, equalled the average reduction in body weight, as *measured* directly on the flight balance. Similarly, the average thrust of the wings corresponded to the drag of the body. The analysis shows how the aerodynamic forces vary *during* the wing stroke.

The hindwings are responsible for about 70 % of the total lift and thrust. About 80 % of the lift is produced during the downstroke. During flight at normal lift the angles of attack (middle part of wing) are small during the upstroke and vary between 10 and 15° during the downstroke. When the lift was larger or smaller than the body weight these figures increased or decreased respectively. The forewings are peculiar in two ways: (i) during the middle part of the downstroke a true flap (the vannus) is put into action; (ii) during the upstroke the proximal part has a Z-shaped cross-section and gives but little lift and drag. The hindwings are characteristic in that the posterior part (vannus) is flexible and becomes moulded by the wind, increasing the angle of attack at which stalling occurs to about 25°.

Since both the movements of the wings relative to the body and the aerodynamic forces are known at any instant, the exchange of power with the surrounding air can be calculated. The moments of inertia of the wing mass being known, the power for accelerating the wings can also be estimated. The sum of these contributions is the power which passes the wing fulcrum; this estimate is used in a later paper (part IX) where the energetics of flight is discussed in detail.

The diagrams are correct to scale.

The restriction of freedom caused by the suspension is discussed, together with the possible errors of a stationary analysis.

1. Introduction

The kinematics of natural flapping flight is so complicated that we cannot expect to understand the dynamics and energetics without a detailed knowledge of the movements and forces during the wing stroke of a normally flying animal. Much too often measurements have been confined to a few of the conspicuous wing-stroke parameters which, when supplemented by various theoretical assumptions, have led to confusing or contradictory results, as has been discussed in part I. For instance, it has repeatedly been claimed that some insects would be unable to lift themselves if only steady-state aerodynamic principles were reckoned and that other forces must contribute to the lift (cf. part I, and Osborne 1951); but neither the nature nor the magnitude of such 'hidden' forces are clear. Factual knowledge of the variation in time of the torque about the wing hinge is virtually non-existent for insects, birds and bats. The purpose of this investigation was to give a detailed,

empirical description of how the wings move through the air in a desert locust (*Schistocerca gregaria*) performing typical forward flight. Based upon this fundamental knowledge, the aerodynamics could be studied when one assumed that steady-state principles could account for the flight and, this being found to be the case, the torque contributions due to wind and mass forces could then be calculated.

Emphasis was laid upon a detailed analysis of horizontal flight at constant speed, excluding all problems of stability and control. Even with this limitation, a quantitative estimate demands a large body of observations whose further treatment is very complicated. With a reasonable amount of labour only a few flight situations could be studied, each comprising a few wing strokes.

Thus four experiments were analyzed in detail. Two of them (nos. I and II) were representative of steady, horizontal flight at normal lift; the locust in no. III lifted considerably more than its body weight while that in no. IV lifted considerably less. It might appear unwise to apply the results obtained from such a small material. However, the four stroboscopic slow-motion films used were selected from a large number of similar films, the selection being based upon an extensive study of the normal spectrum of flight parameters which could easily be measured (Weis-Fogh, part II).

The movement of the wings in space was calculated from measurements of the slow-motion film (Kinematics of the wings). The relationship between the angle of attack, the drag and the lift of the isolated wings was measured in a special wind tunnel where the wind speed increased from base to tip in much the same way as during flight (Aerodynamics of the wings). By means of the polar diagrams thus obtained the aerodynamic forces could be estimated (Dynamics of the flight). Finally, the aerodynamic forces and the forces caused by acceleration of the wing masses were calculated for each of the fifteen to twenty flash exposures representing one wing stroke; these results were used for an estimation of the torque and power in flight (Results and Discussion).

2. Material and methods

(*a*) *Material*

The locusts (*Schistocerca gregaria* Forskål) were bred at the Anti-Locust Research Centre, London, and belonged to phase *transiens* or *gregaria*. (For a detailed account, see Weis-Fogh (1952), who gave indices for the dimensions of the locusts.)

(*b*) *Procedure*

The cinematographic material comprised four stroboscopic slow-motion films selected from a large number of exposures (Weis-Fogh, part II). From an extensive analysis of the correlation between the resultant lift and flying speed and a number of selected wing-stroke parameters, it was possible to compare a given performance with what could be considered the normal combination of quantities.

The data which were used for the present aerodynamic analysis are summarized in table III, 1. The table gives the average values for similar flight performances of locusts of the same size. The lift is expressed as a percentage of the basic weight of the animal, 'relative lift' (see Weis-Fogh, part II).

PHILOSOPHICAL TRANSACTIONS OF THE ROYAL SOCIETY B BIOLOGICAL SCIENCES

If values not deviating from the average by more than the standard deviation, s.d., are denoted by *n*, deviations not exceeding 2 s.d. by + (bigger) or − (smaller), and deviations greater than 2 s.d. by ++ or − −, table III, 2 is obtained.

It is seen that, in general, the quantities from the four selected films are slightly higher than the values found during prolonged, steady flight when the animal flew in complete flight posture. But in the performances I and II where the lift was close to 100 %, the flight parameters were either normal or only insignificantly increased. These flights were

TABLE III, 1. THE FOUR FLIGHT EXPERIMENTS

flight no.	I			II			III			IV		
animal/index of volume	♀*a* 65·8			♂*b* 53·2			♂*c* 46·4			♀*a* 65·8		
relative lift (%)	97 ×			111 *			162 *			70 ○		
	found	normal		found	normal		found	normal		found	normal	
		av.	s.d.		av.	s.d.		av.	s.d.		av.	s.d.
stroke frequency (min^{-1})	1050	990	50	1100	1060	50	1275	1130†		1090	960	60
stroke angle: ϕ_1 (deg.)	83	68	12	79	68	8	68	65‡	10‡	93	70	11
ϕ_2 (deg.)	110	109	7	99	111	6	108	112‡	6‡	105	109	10
middle position: γ'_1 av. (deg.)	105	90	9	105	95	6	86	94‡	7‡	102	83	3
γ'_2 av. (deg.)	95	88	3	93	89	4	92	89‡	3‡	106	86	4
flying speed ($cm\ s^{-1}$)	350	340	40	360	360	50	320	370‡	30‡	320	300	40

○, no hind tibia bent up.
×, one hind tibia bent up.
* both hind tibiae bent up.

† estimated by extrapolation.
‡ the values correspond to 140 % lift.

Suffix 1 = forewing; suffix 2 = hindwing.

TABLE III, 2. THE DEVIATIONS OF THE FOUR FLIGHT PERFORMANCES FROM THE NORMAL

flight no.	I	II	III	IV
flying speed	*n*	*n*	−	*n*
frequency	+	*n*	++	++
stroke angle: ϕ_1	+	+	*n*	++
ϕ_2	*n*	−	*n*	*n*
middle position: γ'_1 av.	+	+	*n*	++
γ'_2 av.	+	*n*	*n*	++
flight posture	×	*	*	○

n = normal = mean value ± s.d.
+ or −, within *n* ± 2 s.d.
++ or − −, beyond *n* ± 2 s.d.

○, no hind tibia bent up.
×, one hind tibia bent up.
* both hind tibiae bent up.

therefore selected as representing normal, horizontal flight. No. III was chosen in order to analyze a typical situation where a high lift was combined with a low forward speed, i.e. a case which might represent the maximum performance of the wing system. No. IV, however, apparently gives the opposite extreme, but it is seen that most of the wing-stroke parameters deviated considerably from the values normally found at 70 % lift. The animal was the same as in no. I, and were it not for the comparison with the average figures as well as for the fact that the locust had not raised its hind tibiae, the regular and symmetrical wing strokes would indicate that the performance was typical for flight with a low lift. The analyses in the following sections will make it clear that performance no. IV must be considered to be an example of 'flight' which has no counterpart in natural

flight. This example stresses the importance of a very careful selection of the situations to be analyzed, and it was chosen as such in favour of a typical low-lift performance since the production of low lifting forces is of little aerodynamic interest.

(*c*) *Experimental technique*

The kinematics of the wings were calculated from slow-motion films of locusts flying in the apparatus shown diagrammatically in figure III, 1. (For further details see part II, appendix B.)

The experimental animal *S* was suspended from a bar *P* and was flying against a current of air from the wind tunnel *WT*. The motor M_1 of the wind tunnel drove an axial compressor *AC* producing an air current. It was controlled through an infinitely variable gear *G*. The air stream flowed through a diffusor to the honeycomb *HC* which was followed by a contraction. At the outlet *N* the air current escaped as an approximately turbulence-free jet with a diameter of 15 cm.

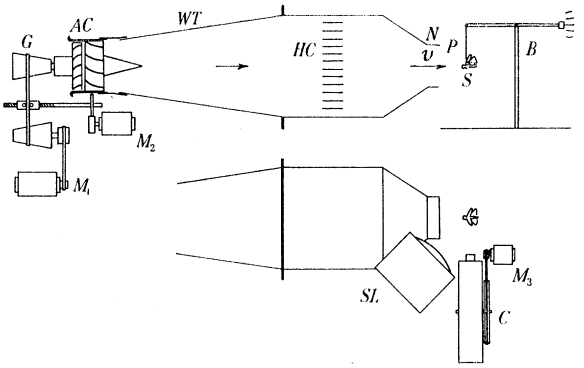

FIGURE III, 1. Schematic illustration of installation used for the slow-motion exposures. The animal flies in an air current from the wind tunnel *WT*. The animal's lift is measured with the balance *B*. The suspension bar *P* is allowed to turn freely about its upper end, and the air current is regulated so that *P* is kept vertical, i.e. the air speed is equal to the flying speed.

The bar *P* from which the animal was suspended constituted the arm of a pendulum turning freely in the vertical plane, i.e. the plane containing both the velocity and the longitudinal axis of the animal. During the experiment, the velocity of the air current was continuously regulated so that *P* was kept vertical, i.e. the velocity equalled the flying speed of the animal. This regulation took place automatically by means of switches on *P* connected with the motor M_2. The bar was placed at one end of the lever *B* and the weight of the animal was compensated. The lift actually produced during the flight was read directly on a calibrated scale.

During the experiment the animal was illuminated by a flash lamp *SL* of high light intensity (General Radio Co. 'Strobolux') which was driven by a stroboscobe with adjustable flash frequency (General Radio Co. 'Strobotax').

The film was taken with a camera *C*, the horizontal axis of which was perpendicular to the direction of flight. The camera was provided with a drum of circumference 100 cm on which was placed a strip of film. The drum was kept at a constant speed of rotation by the motor M_3. The shutter remained closed until it was ascertained that the animal was

flying as naturally as possible judging by its speed, stroke frequency and posture. The shutter was then opened, and after a time interval corresponding to one rotation of the drum it was automatically shut. During the exposure the flash frequency was kept slightly lower than the frequency of the wing stroke. The number of pictures amounted to fifteen to twenty per apparent wing stroke. Altogether there would be about seventy pictures on a strip. (For further details see part II.) Special methods will be described in the following sections.

(*d*) *Degrees of freedom and restriction*

During the experiment, the locust was deprived of some degrees of freedom possessed by animals flying in nature, and these must therefore be discussed.

An insect in natural flight has six degrees of freedom for its bodily movements. A freedom of motion as comprehensive as that would make detailed observations difficult. Summary observations of flying insects are difficult to interpret and hardly adaptable to a quantitative analysis. It therefore seemed evident that the best method would be to deprive the animal of a certain part of the freedom of motion and thus create conditions for measuring. The degrees of freedom to be locked during the experiments had to be chosen with due consideration of their quantitative 'importance' to the animal, i.e. the extent to which the locust could be expected to make use of them. The importance of the various degrees of freedom may be judged from the force or torque acting in that degree of freedom, or by the corresponding work.

The three translational degrees of freedom may be characterized by the aerodynamic forces produced by the wing stroke: the thrust, the horizontal cross-force and the lift; the second of these may be regarded as insignificant. The three rotational degrees of freedom may likewise be characterized as: rolling, pitching and yawing. During the present experiments the animal was allowed to choose its flying speed freely; in addition, the lift was under control and the body angle was adjusted to the lowest value at which the particular insect could perform steady flight.

Each degree of freedom could, of course, be expressed by the acceleration of the motion in question, and the above arguments will only hold provided that the motions are appropriately slow. If they are rapid, i.e. taking place with a frequency similar to that of the wing stroke, the freedom of the locust would be considerably reduced, since the comparatively great mass of the suspension bar would also have to be accelerated. Thus, during the experiment, variations in thrust and lift during each wing stroke would involve a restriction, since the suspended animal could not respond to them by moving to-and-fro and up-and-down respectively; there is a similar restriction in pitching. The quantitative significance of the limitation caused by such rapid changes could to a certain extent be estimated from the experimental results, as is seen on pp. 537 to 541.

3. The wings

(*a*) *Forewings*

Viewed from above the contours of *Schistocerca gregaria* are as shown in figure III, 2. The aspect ratio of the forewing is 5·6.

As in the case with the other parts of the skeleton the forewings of different locusts are very nearly geometrically similar. The area of the wing A may be calculated with fair

approximation as a constant multiplied by the square of the length L of the wing. For the results given here the simple but more accurate formula, $A = cLB$, was used, where B is the maximum chord of the wing. The coefficient c is 0·85. The area of one forewing of the standard animal is 4·85 cm^2. The weight of the forewing is $2{\cdot}16 \times 10^{-3}\ (LB)^{\frac{3}{2}}$ g, L and B being measured in cm, and its moment of inertia of the mass with respect to the wing base is $2{\cdot}81 \times 10^{-8} L^5$ g cm s^2, L to be measured in cm (see Weis-Fogh, part VI).

A section of the wing consists of rings (sections of the veins) connected by thin portions (sections of the membranes). In figure III, 2 is shown part of section c_2. Over the whole section the veins project on an average 0·003 cm from the membranes. Closer to the fulcrum they project still more. In section A the average projection is about 0·007 cm.

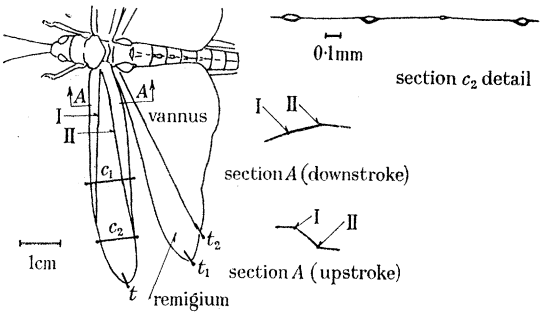

FIGURE III, 2. *Schistocerca gregaria* with unfolded wings. The forewing is rigid but, during flight, it is bent sharply along the lines I and II as shown in the sections. During the first half of the downstroke the wing is flat. The sector of the hindwing (remigium) shown in front of t_2 is rigid, whereas the rest of the wing is rather flexible. The markings used for experiments consisted of thin hairs glued on to the wings and provided with a bead of white painting at the ends. The hair was cut at the hinge lines. I = medial fold; II = vannal fold (see Weis-Fogh, part VI).

The significance of these veins with regard to aerodynamics will be evident when the projections are compared with the thickness of the laminar sublayer. The thickness of the laminar sublayer may be calculated from

$$\delta_{\text{lam.}} = 3{\cdot}4 \sqrt{\frac{\nu}{v}} \sqrt{x}$$

(see e.g. Wien & Harms, *Handbuch der Experimentalphysik*, 1). ν is the kinematic viscosity of the air, v is the velocity of the air current outside the boundary layer and x is the distance from the leading edge of the plane. If $\nu = 0{\cdot}15$ and $v = 500$ cm/s the result will be

$$\delta_{\text{lam.}} = 5{\cdot}9 \times 10^{-2} \sqrt{x}.$$

The projection of the majority of the veins of the wing is 0·007 cm, and the same thickness of the boundary layer exists at a distance of 0·014 cm from the leading edge of the plane. Even if the formula for the calculation of the boundary layer presumes a plane surface which the wing is not, it can give the order of thickness of the boundary layer, and it will be seen that practically all the veins are inside the laminar sublayer and consequently the aerodynamic functioning of the wing will be like that of a smooth surface.

The forewing can be bent sharply along the two lines designated I and II in figure III, 2. During flight there is a bend along line II during the downstroke, and throughout the upstroke the wing is bent along both I and II (see figure III, 2, sections A).

(*b*) *Hindwings*

The form of the fully unfolded hindwing as seen from above is shown in figure III, 2. The area of the hindwing may be expressed by 0·36 L^2, L being the overall length of the wing.

Observations have shown that the forewing is so stiff that it is only slightly deformed by the loads encountered during flight, but the conditions for the hindwing are quite different, since its form, during flight, to some extent depends on the loads encountered.

During the wing stroke the angle between the leading edge of the hindwing and the longitudinal axis of the animal varies. It reaches its maximum at the lowest point of the downstroke where it slightly exceeds 90°, whereas it is only 60° at the top position. This variation is brought about by the wing being folded only at the inner margin parallel to the body, while otherwise remaining extended. If not quite fresh, isolated wings will fold along *all* existing folds when the angle is decreased.

4. Kinematics of the wings

(*a*) *Analysis of the film*

Each flight experiment comprises a series of about seventy equally spaced photographs, which with slow motion can be seen to cover three to five wing strokes. The wings were marked as indicated in figure III, 2. The forewing was marked at the tip t, and was further provided with two hair-lines c_1 and c_2 indicating its position in space. The inner line c_1 was placed so near to the fulcrum that it crossed the distal part of the vannus; the hair was cut through at the vannal fold so that the bending of the vannus flap against the remigium was unhampered and could be estimated.

The hindwing was provided with two indicator points t_1 and t_2. As far as the front sector (remigium) was concerned, twisting of the wing could be deduced from the markings, but they did not make it possible to determine the shape of the vannus. However, an aerodynamic analysis has shown that the shape of this part of the wing influences flight in such a manner that it is unnecessary to have a detailed knowledge of it in order to estimate the aerodynamic forces.

(*b*) *Elementary movement of the forewing*

The complicated translatory movements of the base of the forewing are of insignificant magnitude; the main movement of the forewing consists of a turning about a point *fulcrum*. Thus the movement of the wing tip is restricted to a spherical surface, the centre of which is the point of attachment to the thorax and the radius of which is the length of the wing.

The movements of the wing tip on this spherical surface are rather complex, and a description of the kinematics of the wing is further complicated by the fact that the movement must be considered in relation both to the animal and to the air through which it is flying. Finally, the turning of the wing in relation to the animal and the twist of the wing have to be taken into account. In order to understand the kinematics of the wings it is necessary to consider these points in turn and to show the movements in several reference systems.

Figures III, 3 to III, 10, which all derived from flight I, show the movements of the wings in the co-ordinate systems used.

PHILOSOPHICAL TRANSACTIONS OF THE ROYAL SOCIETY B BIOLOGICAL SCIENCES

The co-ordinate system of the animal

It is simplest to begin with the movements of the wing tip. If it is thought desirable to have a representation of the wing it may be represented by a straight line from the fulcrum to the tip. The wing is placed in a rectangular right-hand co-ordinate system *XYZ*, the origin of which is fixed in the fulcrum, and the *X*-axis is in the direction of flight (i.e. horizontal and parallel with the plane of symmetry of the animal and positive in the forward direction in relation to the animal). The *Z*-axis is positive in the upward direction

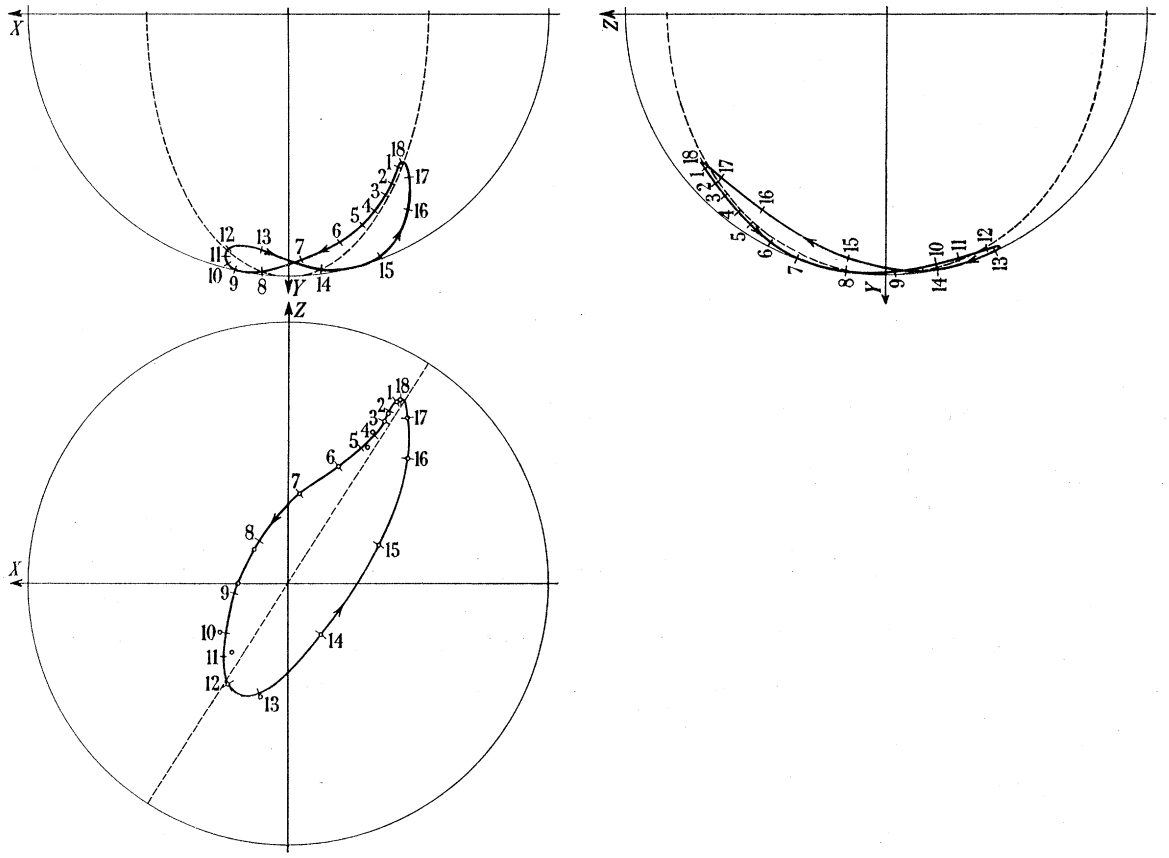

FIGURE III, 3. Movement of the wing tip in relation to the animal. *X* is forward, *Y* horizontal to the left of the animal and *Z* upward; the origin is the fulcrum. Points denoted by a circle were measured on slow-motion films; points denoted by cross-lines on the curves are the corrected values. The time interval between the points was $3{\cdot}3 \times 10^{-3}$ s.

and the *Y*-axis is positive to the left of the animal (this and the following descriptions refer to the wings of the left side). This co-ordinate system is called the co-ordinate system of the animal, and it is in this system that the wing tip is moving as on a spherical surface.

The origin was indicated on each photograph. When the forewing is above the horizontal plane, the fulcrum is seen plainly; in other positions it is easily located by means of the veins. The photographs being provided with a horizontal line of reference the *X*- and *Z*-axes of the co-ordinate system of the animal could be drawn on the copy. The two corresponding co-ordinates of the wing tip were then determined by direct measurement and the *Y* value was calculated from these and the true length of the wing. All co-ordinates were corrected with respect to the perspective.

The animal's co-ordinate system may be represented by three two-dimensional systems XY, YZ and ZX. If the co-ordinates of the wing tip for two or three apparent wing strokes are plotted, the points will be located so that a proper curve of the movements may be drawn in each of the three systems. The points, however, are not all located on the curve. This is due partly to inaccuracies of measurement and partly to the fact that each successive exposure in a stroboscopic series is derived from the succeeding wing stroke. Even if the wing beat is highly regular it is not exactly the same from one stroke to the next. Finally, it should be noted that the flashes from the stroboscope are not always precisely equidistant with regard to time, a fact which could be seen from parallel time recordings (50 c/s) on the film.

By means of the curves of movement a correction was made of the points derived from the single wing strokes so that those located outside the curve were transferred to it. Further, the placing of the points in the curve was corrected for the discrepancy in the time intervals of the photos.

The result is shown in figure III, 3. The points representing the primary observations are marked by small circles in the ZX-plane, and the corresponding corrected points are shown by cross-bars in the curves. The large circles represent the intersections between the sphere of the wing tip and the co-ordinate planes. The serial numbering of the points indicates the time, the time interval being $3{\cdot}29 \times 10^{-3}$ s.

The co-ordinate system of flight

The animal was flying in an air current or, from another point of view, it was flying at a certain speed in still air. In flight no. I the equivalent speed of flight was 350 cm/s, and the animal thus effectively advanced through the air 1·15 cm between two successive photographs. The movement of the wing tip in relation to the air was calculated from the movement in the animal's co-ordinate system by adding in the direction of X 1·15 cm constituting the translation per exposure.

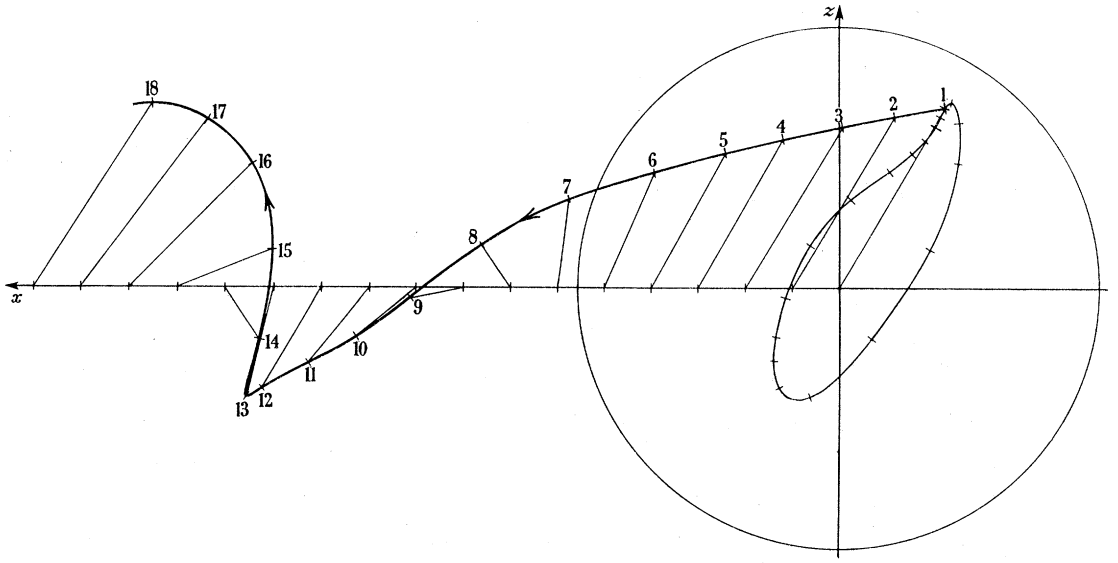

FIGURE III, 4. Movement of the tip of the forewing in relation to the air. x is the direction of flight, z is upward. A repetition of the curve from figure III, 3 is seen to the right. The x-axis with the division lines shows the movements of the fulcrum.

This rectangular right-hand co-ordinate system *xyz* is called the co-ordinate system of flight. The origin is fixed relative to the air at the point where the fulcrum was located when photo no. 1 was exposed. The axes of *x*, *y* and *z* are congruent with the corresponding axes *X*, *Y* and *Z* of the animal's co-ordinate system at the arbitrary initial point.

Figure III, 4 shows the curve of movements in the *zx*-system with the curve of movement from the *ZX*-system inserted to the right. Since the movement of the animal's co-ordinate system in relation to the co-ordinate system of flight is only a translation in the direction of *X*, the projection of the curve of movement on the *yz*-plane will correspond to the projection on the *YZ*-plane. The projection of the curve on the *xy*-plane has little interest.

It should be noted that the diagrams are plane projections of the true curve of movement in space and, therefore, they do not directly allow measurements to be made of parameters such as the velocity of the wing tip, even if they are provided with a parameter of time (the serial numbers of photographs). Since the movements take place on a surface that cannot be developed, no exact method of representation on the plane exists which will give true values. However, for the present purpose the following systems were sufficient.

The ΦΓ-system

In the *ZX*-plane it will be seen (figure III, 3) that the closed curve of movement is markedly elongated, and inclined about 30° to the *Z*-axis. On the sphere a great circle can be inserted which follows the path of the wing tip 'as nearly as possible'. In the present case it is the great circle in the plane containing the *Y*-axis; in other cases the

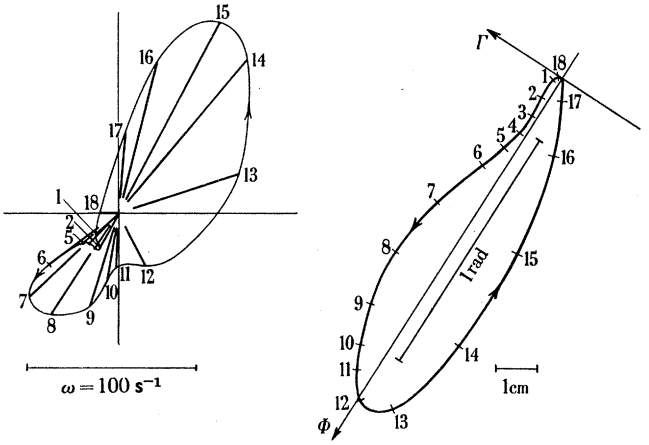

FIGURE III, 5. Right, the developed picture of the movement of the tip of the forewing in relation to the animal. Left, hodograph for the movement of the forewing.

plane has a small inclination to the *Y*-axis. In figure III, 3 the great circle is represented by broken ellipses in the *XY*- and *YZ*-planes, and by a straight line in the *ZX*-plane.

The curve of movement of the wing tip was projected on a circular cylinder touching the sphere at the great circle referred to. On account of the elongated form of the curve, it is restricted to a rather narrow strip of the cylindrical surface. When developed this surface contains a representation of the curve of movement of the wing tip which is of correct proportions apart from the errors produced by the projection from the sphere to the cylindrical surface. The errors are biggest for those parts of the curve which are most

removed from the great circle, and they correspond to the difference between the length of an arc to a point on the sphere (measured from the great circle) and the distance to the projection of the corresponding point on the cylindrical surface (measured along a generator).

Figure III, 5, right, represents the wing action in this development. The co-ordinate system has its Φ in the developed great circle, and the origin is the upper intersection of the great circle with the curve representing the path of the wing tip. The other axis is the generator of the cylinder in the origin. In this reference system the movement of the wing tip on the surface of the sphere may be viewed directly, and true values of the velocity of the wing tip as well as the angular velocity and acceleration of the wing may be measured, but it is not possible to obtain true values of the acceleration of the wing tip as the component of the acceleration in the radius vector is missing.

The $\phi\gamma$-system

On the *xyz*-system, which is fixed in the air, the movement of the wing tip will very closely resemble an ellipse when projected in the direction of x; this ellipse is the projection of the great circle on the *yz*-plane. With certain approximation the wing tip during flight will follow the surface of an elliptical cylinder with generators in the direction

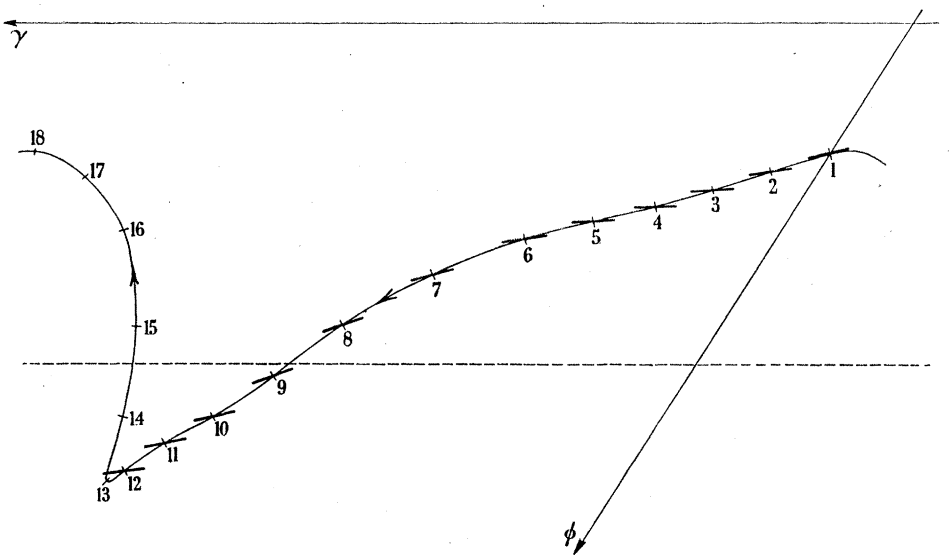

FIGURE III, 6. Developed picture of the movement of the forewing in relation to the air. The heavy lines at the division points indicate the position of the tangent plane of the wing at the wing tip.

of x. A development of the surface of this cylinder gave the curve of movement shown in figure III, 6, which, with certain reservations, shows the true movement of the wing tip through the air. The reservations are related both to the production of the development of the axes of Φ and Γ, and to an error (numerically larger) due to the fact that the wing tip follows the elliptical cylinder of the *xyz*-system to a lesser degree than it follows the circular cylinder of the *XYZ*-system; in other words, as regards both its indicatrix and the direction of its generator the circular cylinder is suited in the best possible way, whereas the elliptical cylinder must have the x-axis as the direction of the generator.

(*c*) *The twisting movements of the forewing*

During the complete wing stroke the inclination of the base of the forewing with the longitudinal axis was practically constant, and equalled the body angle B (part II) which was known.

Apart from this, the wing was twisted during the downstroke so that the leading edge was lower than the trailing edge, and during the latter part of the downstroke the cross-section of the wing was further bent along the rear hinge line (vannal fold). During the upstroke the distal part of the wing was twisted so that the leading edge was raised and the proximal part was both twisted and bent along both hinge lines (see figure III, 2). Further details of these twistings will be given in a later paper (part VI).

Photographic measurements have proved that apart from the Z-form of the proximal wing sections during the upstroke the angle of twisting was always constant per unit of length; this was seen from transverse marking on the outer part of the wing. Owing to the linear twist, the form of the surface has only one parameter. For this purpose it was expedient to use a reference line at the wing tip defined as a line perpendicular to the axis of the wing and placed in the tangent plane to the wing at the tip.

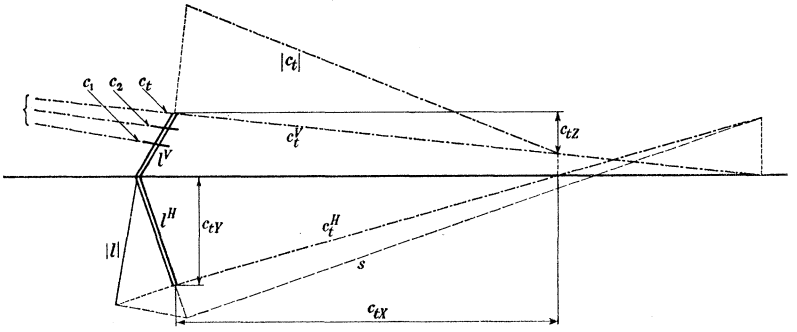

FIGURE III, 7.

The various positions in space of this cross-line were obtained by a geometrical construction upon the ZX- and the XY-planes. In figure III, 7, l^V and l^H are horizontal and vertical projections respectively of the axis of the wing, where l is the line from the fulcrum to the indicator point at the tip. $|\,l\,|$ is the true length of this line when turned to the XY-plane about l^H. When corrected for the distortion of the perspective the vertical view will be the same as the photographs showing the transverse markings c_1 and c_2. The twist of the wing surface from c_2 over c_1 to the wing tip being small, the vertical projection of the cross-line through the wing tip c_t may be extrapolated as shown in the figure.

In the XY-plane a plane normal to the axis l of the wing was laid through the wing tip t, s being the intersecting line between this plane and XY-plane; the cross-line c_t through the wing tip must be contained in this plane. Then the horizontal projection c_t^H was obtained as shown in the figure from the track of c line in the two co-ordinate planes. Finally, the true length $|\,c_t\,|$ is determined by turning c about its vertical projection to the ZX-plane.

In the further treatment, which is analytical, the inclination of c was determined in relation to the axis of the co-ordinate system of the animal ($c_{tX}c_{tY}c_{tZ}$).

(*d*) *The kinematics of the forewing fitted for aerodynamic analysis*

The aerodynamics of the wing (including the aerodynamic forces on the wing in a given position during the wing stroke considered in relation to the medium) depend on the instantaneous movement of the wing in the medium. If the matter is regarded in relation to the wing, it is a problem of the velocity field about the wing. The action of the forces on a fixed wing in an air stream is dependent on the velocity of the undisturbed flow and of the attitude of the wing. With a flying animal, the problem is more complicated as the relative velocity changes both in value and direction from point to point along the axis of the wing.

It is of course possible to undertake a two-dimensional analysis for any cross-section of the wing. The only parameters will be: the velocity of the wind v, the angle between the wind velocity and the longitudinal axis β, and the angle between the wind velocity and the chord plane to the wing. For reasons indicated below, the third parameter was replaced by the angle between the cross-line of the wing surface at the point under consideration and a plane determined by the wind velocity and the axis of the wing. This angle is referred to as the angle of attack α.

On account of induced velocities, however, it would be very difficult to calculate the resultant forces on the wing from a series of such two-dimensional analyses. Apart from the case where the induced downwash is constant at all cross-sections no simple methods are known for the calculation on the basis of two-dimensional measurements of the forces on a surface surrounded by air flowing in three dimensions. In the present analysis it was considered preferable to solve the problem of the induced drag by measuring the forces on a whole wing which was submerged 'best possible'. The relation between the kinematics and aerodynamics was established by means of the values of the three parameters mentioned above (v, β and α), all being calculated for the tip, the middle and the base of the wing. This was achieved by vector analysis. The axis of the wing was the vector $\mathbf{l}$ and was known (by its co-ordinates in the animal's co-ordinate system) in a series of time-equidistant situations during a wing stroke. The velocity of the wing tip could now be calculated from $\mathbf{l}$ at an arbitrarily chosen time by dividing the mean values of the differences $\mathbf{l}_{n+1}-\mathbf{l}_n$ and $\mathbf{l}_n-\mathbf{l}_{n-1}$ by the time interval. In the special cases of the upper and lower wing positions, where the accelerations were considerable as the wing tip was moving on its sphere in less circles of small radii, the 'chord computation' of the velocity of the wing tip must be modified. This was easily done by using the tangents of the curve movement in the developed views.

The velocity of the extreme point of the $\mathbf{l}$ vector thus calculated must be converted to the co-ordinate system of flight by adding the forward velocity of the wing tip in the co-ordinate system of flight. The angle β made by the axis of the wing with the velocity of the wing tip is obtained from the scalar product of the two corresponding vectors

$$\cos\beta=\frac{\mathbf{l}\,.\,\mathbf{v}}{lv}$$

and will be considered positive from $\mathbf{l}$ to $\mathbf{v}$. The angle of attack α depends *inter alia* on the twisting of the wing. The cross marking c_t was regarded as a vector $\mathbf{c}_t$, considered positive

from the trailing to the leading edge of the wing. The angle of attack was defined as the angle between $\mathbf{c}_t$ and the plane containing $\mathbf{v}$ and $\mathbf{l}$, in practice calculated from the normal $\mathbf{n}$ of the plane and $\mathbf{c}_t$.

The normal $\mathbf{n}$ to the plane containing $\mathbf{v}$ and $\mathbf{l}$ is the vector product of the two vectors $\mathbf{n}=\mathbf{v}\times\mathbf{l}$. The sign of $\mathbf{n}$ is determined by $\mathbf{v}$, $\mathbf{l}$ and $\mathbf{n}$ being a right-hand system. The angle between the normal vector and the cross-line is $\frac{1}{2}\pi-\alpha$, α being the angle of attack, and it can be calculated from the scalar product of the two vectors

$$\cos\left(\tfrac{1}{2}\pi-\alpha\right)=\frac{\mathbf{n}.\mathbf{c}}{nc}.$$

In the developed view of the curve representing the path of the wing tip (figure III, 6), α is indicated by the acute angles between the wing path and the heavy lines. This figure gives a fair idea of the movement and especially of the twisting at the wing tip, but it should be noted that it is not strictly correct. By means of a similar analysis v, β and α were determined for the mid-point and for the base. Figure III, 8 shows the path of the mid-point, the plane of the wing being indicated. At the base the movement of the wing was simple because the angle of attack was constant.

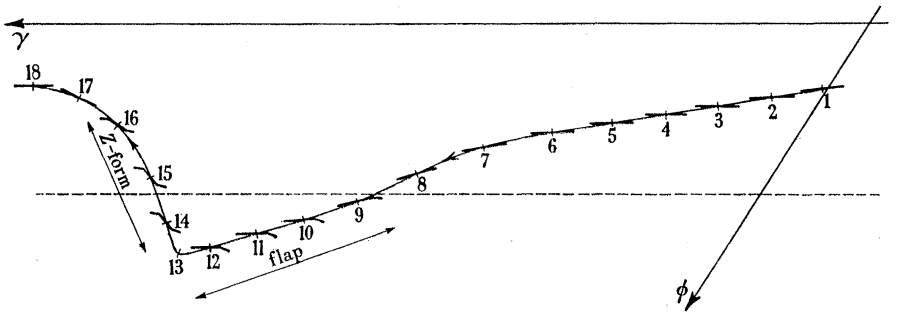

FIGURE III, 8. The movement of the mid-section of the forewing in relation to the air. The section is shown at each division point. From 9 to 12 the flap is active. The Z-form section during the upstroke should be noted.

(e) *The elementary movement and the twist of the hindwing*

The movements of the tip of the hindwing resemble those of the forewing. Figure III, 9 shows the movement in the animal's co-ordinate system; the origin and axes are the same as before, but the centre of the sphere of the wing tip is placed in the fulcrum of the hindwing, i.e. behind and somewhat lower than that of the forewing. As in the forewing, the tip of the hindwing is travelling near a great circle on the sphere as shown by the broken line in figure III, 9. The movement of the hindwing in the co-ordinate system of flight is shown in figure III, 10, where the movement of the forewing also is indicated.

It appears from figure III, 10 that, in general, the movements of the tips of the two pairs of wings resemble each other; in relation to the animal they consist of a slow forwardly inclined downstroke and a fast backward upstroke. In both wings the speed of the backward movement during the upstroke is equal to the flying speed. At the start of the upstroke it even exceeds the flying speed, so that the tips are moved backwards through the air. This of course only applies to the distal parts of the wings.

The movements of the two wings differed in other respects. In the experiment under consideration the time interval between the top positions was $0{\cdot}11\,T$ (T is the time for a complete wing stroke), during the middle of the downstroke it was $0{\cdot}23\,T$, in the lowest positions $0{\cdot}14\,T$, and during the middle of the upstroke $0{\cdot}05\,T$. The hindwing is always ahead of the forewing.

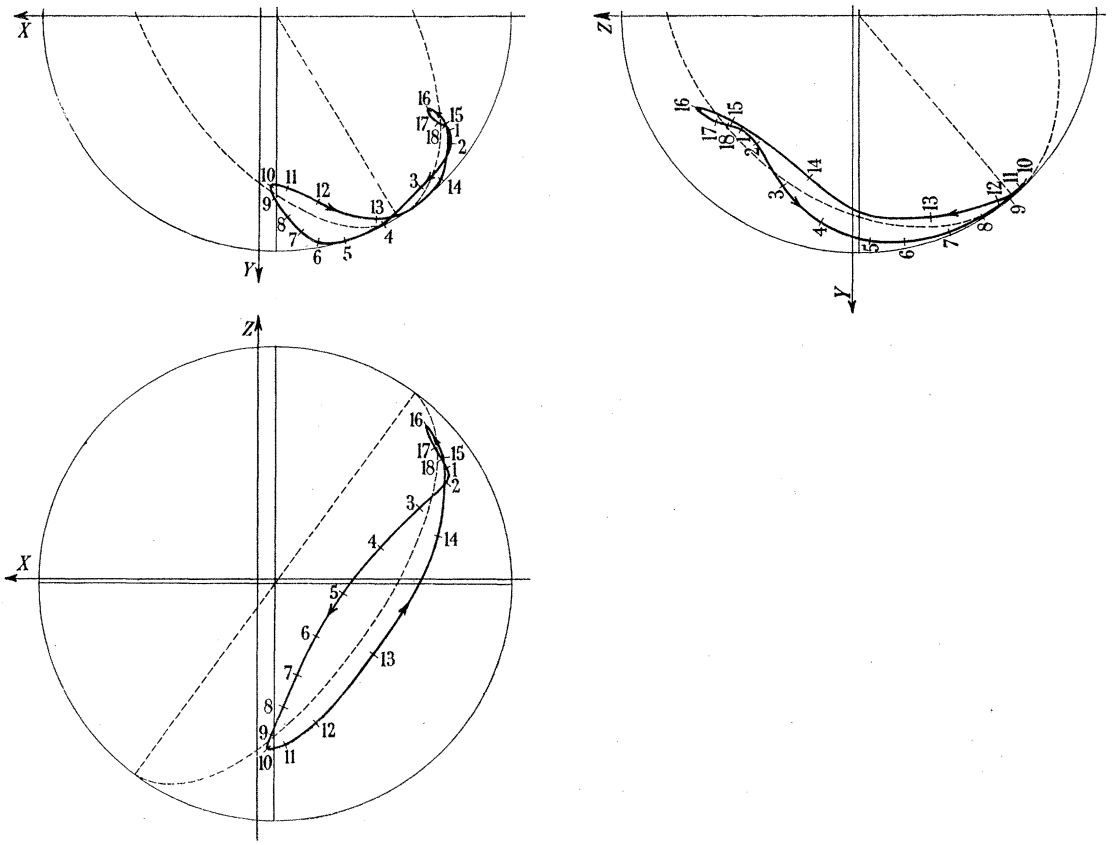

FIGURE III, 9. The movement of the tip of the hindwing in relation to the animal. X is forward, Y is horizontal to the left of the animal, Z is upward and the origin is the fulcrum. The numbering of the points corresponds to figure III, 3.

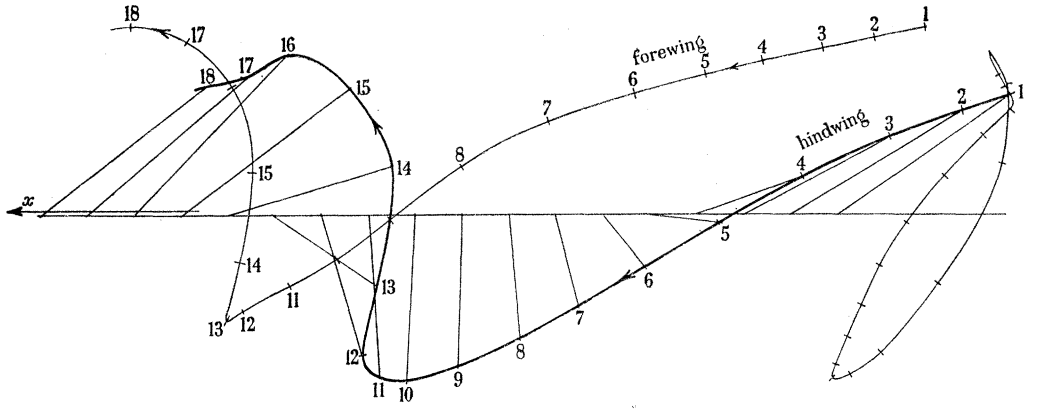

FIGURE III, 10. The movement of the tip of the hindwing in relation to the air. x is the direction of flight and z is upward. The heavy line represents the hindwing and the thin line the forewing.

The twisting of the forewing is determined by the thorax, and this was also the case with the front part (remigium) of the hindwing. In the rear part (vannus) of the hindwing, the deformations were also determined by aerodynamic forces. The hindwings being more or less moulded by the air flow itself. Therefore, in an aerodynamic sense, the hindwing differed in principle from a rigid airfoil.

The remigium of the hindwing is supported by groups of fairly stiff veins (t_1 and t_2 in figure III, 2); during flight this part was so well defined that a suitable angle of attack could be defined and calculated. The rest of the hindwing was less simple apart from the proximal part of the vannus where the angle of attack was equal to the body angle B.

(*f*) *The kinematics of the hindwing fitted for aerodynamic analysis*

In the hindwing the velocity v, the inclination of the wing β, and the angle of attack of the remigium α were calculated for the wing tip and for the wing base.

A vector $\mathbf{l}_1$ connected the fulcrum with the anterior marking point t_1 and the vector $\mathbf{l}_2$ ran from the fulcrum to the posterior marking t_2. The co-ordinates of these vectors were computed from the film. The velocity of the extreme point t_1 in the animal's co-ordinate system was computed and v was found by adding the flying velocity.

The angle of the leading edge of the wing (β) in relation to the velocity of the wing tip was given by

$$\cos\beta = \frac{\mathbf{l}_1 . \mathbf{v}}{l_1 v},$$

β being positive in the direction from $\mathbf{l}_1$ to $\mathbf{v}$. The velocity of the wing tip and the vector $\mathbf{l}_1$ determine a plane the normal $\mathbf{n}$ of which was calculated from $\mathbf{n}=\mathbf{v}\times\mathbf{l}_1$. $\mathbf{l}_1$ and $\mathbf{l}_2$ represented the remigium of the wing and determined a plane the normal $\mathbf{m}$ of which was calculated from $\mathbf{m}=\mathbf{l}_1\times\mathbf{l}_2$. The angle of attack α was defined as the angle between these two planes and was calculated from

$$\cos\alpha = \frac{\mathbf{n} . \mathbf{m}}{nm}.$$

In addition, $\mathbf{v}$ and β were also calculated for the wing base, where α was equal to the body angle of the animal.

(*g*) *Numerical example of the kinematic calculations*

(See Appendix 1)

5. Aerodynamics of the wings

The result of the kinematic analysis was a determination of the following parameters for each of the fifteen to twenty positions covering a complete wing stroke: velocity, angle between the long axis of the wing and the air velocity, and the angle of attack. The parameters were calculated for the tip, the middle and the base of the forewing, and for the tip and base of the hindwing. In order to translate this into aerodynamics it is necessary to know the characteristics of the wings over the observed range of values of these parameters.

PHILOSOPHICAL TRANSACTIONS OF THE ROYAL SOCIETY B BIOLOGICAL SCIENCES

(*a*) *Experimental technique*

During the wing stroke the speed of the air varied from the base to the tip of the wing. At the downstroke of the forewing, the variation ranged from 1/1·2 to 1/2 with a mean of 1/1·5. Since the induced drag of an airfoil placed in a graded and continuously changing wind-velocity field cannot be calculated, experimental conditions were designed which would allow a direct estimate to be made of the wind forces.

The measurements of the forces acting on the wings were made in an air current with substantially the same main variations as found during flight. The graded velocity field was obtained by placing the isolated wing inside a limited part of the boundary layer of a wind tunnel. The general characteristics of the tunnel have already been described (Martin Jensen 1954). Figure III, 11, top, shows the working section of the wind tunnel

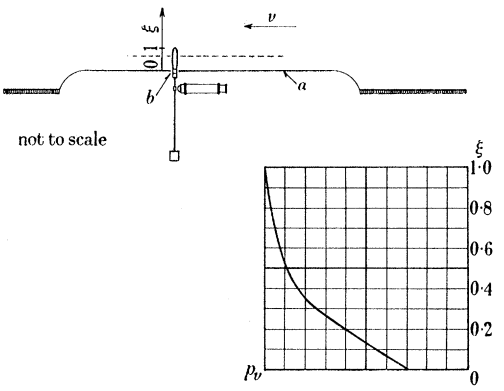

FIGURE III, 11. Measurement of the aerodynamic forces on the wings (schematic). The wing is mounted on the end of a steel bar (at *b*) and protrudes through an aperture in the sheet (*a*) into the wind tunnel. The steel bar supporting the wing at one end is built in at the other end and will be deflected when the wing is exposed to aerodynamic forces. The two components of the deflexion are measured in the microscope. In the lower right-hand corner is shown the profile of the dynamic pressure at the section of measurement. The aim has been to obtain similarity with the variation of the dynamic pressure (from wing base to wing tip) during flight.

as viewed from above. *a* is a smooth metal sheet inserted in the lateral tunnel wall and serving to modify the boundary layer so as to correspond as closely as necessary to the natural wind field of flight. At *b*, the wing passes through a hole in the sheet. The profile of the dynamic pressure at the working section is shown in figure III, 11 below. Since the experiments were made at true wind velocities and with natural wings there were no problems as to model laws.

Fresh wings were fixed at the free end of a steel bar mounted as a cantilever. The aerodynamic force on the wing was determined by its vertical and horizontal components respectively as estimated from the deflexions of the bar. The measurements were made with a microscope and the arrangement is shown schematically in figure III, 11, top. The vertical force on the wing might for example be 0·8 g, and the horizontal force 0·15 g, corresponding to deflexions of 0·065 and 0·012 cm, respectively. The accuracy was about 0·001 cm for vertical and 0·0003 cm for horizontal deflexions, so that the relative accuracies were 1·5 and 2·5 %. The dynamic pressure to which the measurements must be referred was determined to a relative accuracy of 2·5 %. Each result was an average of three

observations, and thus, generally, the relative accuracy of the determinations of each component of force was 3 %.

At the first setting the error of the angle of attack could amount to 1·5°. The succeeding settings did not cause additional errors. The influence of the angle β on the measurements was so small that errors could be disregarded.

(*b*) *The polar curves of the forewing*

The results of the measurements on the whole, unbent forewing are seen in figure III, 12, where the abscissa is the coefficient of drag C_D and the ordinate the coefficient of lift C_L. The angle of attack is indicated on the curves. The full curve corresponds to $\beta = 90°$ (perpendicular to the wind) and the broken curves to other inclinations of the long axis of the wing in relation to the air current. The positive and negative deviations of β from

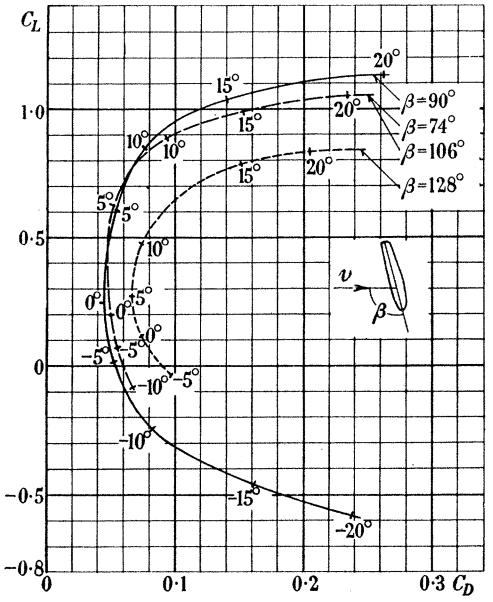

FIGURE III, 12. Polar curves for the unbent forewing in a graded wind field as shown in figure III, 11. The parameters on the curves are the angle of attack.

90° need not be expressed by different curves if the numerical value is less than 16°. At *small* lifts the drag of the forewing was somewhat greater than those of normal airfoils, but apart from this the polar curve for the forewing resembled similar curves from ordinary airfoils.

As already mentioned, during the latter half of the downstroke the forewing bends along the rear hinge line (the vannal fold), making the section convex upwards. The angle of bending was measured on the photographs. In these experiments it was rather constant (about 25°) and appears to be anatomically-mechanically determined (part VI).

Since, towards the end of the downstroke, the angle of attack slightly exceeded its initial value and, in fact, exceeded the value of maximum lift of the unbent wing, the locust makes use of a true flap mechanism.

Figure III, 13 shows the polar curve for the whole forewing with the rear part bent at an angle of 25°. The application of the flap of course increased the lift/drag ratio, but

since it took place during the latter half of the downstroke where kinetic energy should be degraded, extra lift could be produced without any extra cost.

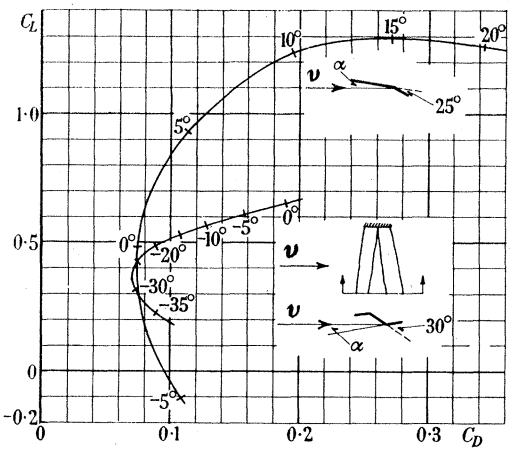

FIGURE III, 13. Polar curves for the whole forewing (big curve) when the flap is set at 25° against the main wing. Graded wind field. The parameters on the curves are the angles of attack. By comparison with figure III, 12 it will be seen that the flap increases the lift. The small curve derives from two-dimensional experiments with the Z-section (during the upstroke).

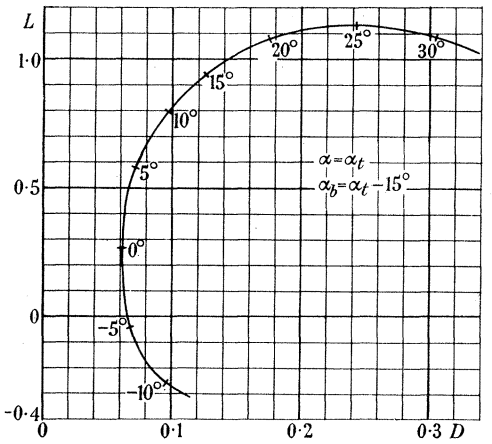

FIGURE III, 14. Polar curve for one hindwing of a standard locust. Abscissa and ordinate: drag and lift in grams at a dynamic pressure of 0·1 cm water column ($v=400$ cm/s). On the curve are indicated the angles of attack at the tip. At the base of the wing the angle of attack at low air speeds is 15° less.

Z-profile

The polar curve for the special Z-section differed from the polar curves of normal aerofoils in that both drag and lift retain moderate values over a surprisingly large field of variation of the angle of attack. The Z-profile was only seen during the upstroke. (For definition of α see lower inset in figure III, 13.)

For the examination of the action of the Z-section during the upstroke, a two-dimensional experiment was carried out with the inner half of a forewing. An additional plane sheet was placed in the wind tunnel at a distance of 3 cm from the sheet *a* and is represented by

the broken line in figure III, 11; this gave a nearly constant velocity profile. At the two walls there was a boundary layer 0·3 cm thick, and the extremities of the wing sector extended into the boundary layers. The results of the measurements of the forces are shown in figure III, 13 (small curve).

(*c*) *The polar curves of the hindwing*

Measurements on the hindwing have shown that lift as well as drag vary so little with β that this angle need not be considered in this connexion. Figure III, 14 shows the polar curve for the hindwing. The abscissa and the ordinate are in grams at a dynamic pressure of 0·1 cm water column. The curve is referred to a standard wing.

6. Dynamics of the flight

It should be possible to calculate the wind forces on the wings during a wing stroke by combining the results given in the polar diagrams with the kinematic analysis. Thus a detailed aerodynamic analysis would result from the kinematic data if the wind forces on the isolated wings were measured for all combinations of parameters described in the preceding chapter, i.e. for all observed combinations of the variation of the parameters from tip to base. However, such an elaborate set of measurements has not been made. The measurements were confined to the possible combinations of values at *one* point on the long axis of the wing while a fixed variation of the parameters was maintained along the axis; the missing situations must therefore be derived from the measured ones by means of theoretical considerations.

(*a*) *Forewings*

Let us first consider the wing tip (suffix t). The angle of attack α_t and the angle of inclination β_t are known at any instant of the stroke, and the corresponding instantaneous coefficients of lift and drag C_L and C_D can be read from figures III, 12, III, 13 and III, 14; consequently, two force components (lift and drag) can be calculated by multiplication with the surface area of the wing A and with the dynamic wind pressure at the tip. These calculated force components correspond to the true instantaneous wind forces on the forewings provided the parameters, which had correct values at the tip, are also correct along the remaining part of the wing. But this was not the case because, during the measurements, α and β were the same at the three points under consideration (tip, middle, and base) and the dynamic wind pressure varied as shown in figure III, 11. The true force components therefore deviate from L_t and D_t. However, the corresponding values of the three parameters (α, β and v) are also known at the middle of the wing m and at its base b, allowing similar calculations of the forces L_m, D_m, L_b and D_b. It should now be possible to estimate the true lift and drag of the wing by making weighted means of the three lift components and the three drag components; but the 2 times 3 force components have different directions, and it is necessary first to make them additive by referring them to a common system.

Summation

By definition the lift coefficient C_L and thus the estimated lift L is contained in the normal $\mathbf{n}$ to the plane given by the two vectors, the long axis of the wing and the wing

velocity. The drag D is perpendicular to L and its direction is opposite to that of the velocity vector. The components of **n** were calculated in the animal's co-ordinate system (X, Y, Z) and from this could be calculated the lift components L_X, L_Y and L_Z and the drag components D_X, D_Y and D_Z. At the tip, for instance, and in the direction of the X-axis, the force becomes $P_{tX}=L_{tX}+D_{tX}$ and so on, giving 3 times 3 components. The components which have the same second suffix (X, Y or Z) are arithmetically additive, and the instantaneous force upon the wing could now be estimated as a weighted summation of these components.

Load integral

Knowing the forces at the tip, the middle and the base of the wing one must, in making a weighted mean, give most credit to the middle point which 'represents' twice as much of the long wing axis as do each of the end-points. It is furthermore reasonable to take the wing width into account because of the broad base and the tapering tip and, finally, one must consider how the dynamic pressure at the given phase of the stroke differs from that during the measurement of the wind forces.

For the present purpose it was found sufficiently accurate to consider the two resulting force components acting upon the wing as proportional to $\int_0^\Lambda p_v(\lambda)B(\lambda)\mathrm{d}\lambda$, where p_v is the dynamic pressure, B the wing width, and the variable λ is zero at the wing base and Λ at the tip. To convert the expression to non-dimensional form it was divided by the surface area $A=\int_0^\Lambda B(\lambda)\mathrm{d}\lambda$ as well as the dynamic wind pressure at the wing tip. The expression thus arrived at was called the load integral. In the forewings it amounted to 0·768 when the dynamic pressure varied as seen in figure III, 11 (situation of measurement).

Weighted mean

During the downstroke the average ratio between the velocity of the wing at the base v_b and at the tip v_t was $v_b:v_t=1:1{\cdot}5$, the variation between them being approximately, although not exactly, linear. When the variation was considered as linear the load integral amounted to 0·666. Otherwise, the ratio varied from 1:1·2 to 1:2·0, and the corresponding load integrals ranged from 0·825 to 0·535.

In the case that $v_b:v_t=1:1{\cdot}5$, the dynamic wind pressure at the base, the middle and the tip would be related as 0·44:0·69:1·00; disregarding the differences in α and β, the previously defined force components would also be $P_{bX}:P_{mX}:P_{tX}=0{\cdot}44:0{\cdot}69:1{\cdot}00$, etc. In this example, which is typical for the downstroke, the weighting factors (i_b, i_m, i_t) are related by $i_b\times 0{\cdot}44+i_m\times 0{\cdot}69+i_t\times 1{\cdot}00=0{\cdot}666$ (=load integral). Considering the found values of $v_b:v_t$ and the 'importance' of the different wing positions for the flight, the following best weighting factors were calculated: $i_b:i_m:i_t=0{\cdot}32:0{\cdot}50:0{\cdot}18$. Theoretically this calculation is free of error when $v_b:v_t=1:1{\cdot}15$; at the other observed values the theoretical error maximally amounted to 1 %.

Z-profile

It was mentioned on p. 517 that the proximal part of the wing in transverse section resembles a horizontal letter Z (Z-profile) during part of the upstroke; the force coefficients

of this special wing profile were measured under two-dimensional conditions (diagram figure III, 13). In the numerical calculation these coefficients were used for the base and the middle part of the wing while the tip was given the values found with 'normally' shaped wings. The above weight figures (0·32:0·50:0·18) were chosen. The calculation is not very satisfactory because the flow round the wing must deviate considerably from the suggested flow. The lift, for example, had opposite directions at the tip and at the middle. However, the approximation was considered as sufficient because of the relatively short time (figure III, 8) during which the Z-profile was being used. A special investigation would be necessary to clear up the details.

(*b*) *Hindwings*

The calculation of the forces proceeded as with the forewings with the exception that no kinematic measurements were available from the middle part of the wing so that the adjustment of the parameters was confined to tip and base. The weight figures were calculated to $i_b : i_t = 0{\cdot}66 : 0{\cdot}34$ corresponding to zero theoretical error when $v_b : v_t = 1 : 1{\cdot}15$, i.e. at normal base:tip ratios. During the downstroke the ratio ranged from 1:1·0 to 1:2·0, giving a maximum theoretical error of 2%. But in a single position during the upstroke the ratio rose to 1:2·5 and the error to 6%. However, the entire calculation comprised eighteen positions, so that it would be of no significance.

(*c*) *Mutual effect of forewings and hindwings*

When a single wing moves, it will create a circulation in the ambient air. This circulation will cause a change in the direction of the air current calculated on the basis of the relative movement of the wing; numerically, the circulation corresponds to an increase of the angle of attack. However, when the lift and the drag are measured at the same uncorrected angle of attack as exists during the flight, no systematic error will be made in the analysis.

However, the circulation about the forewing will also change the conditions of the flow about the hindwing and the circulation about the hindwing will change the flow about the forewing. The qualitative effect when both wings are in the downstroke is that the circulation from the forewing gives a downward velocity component at the locus of the hindwing, corresponding to the hindwing having an angle of attack smaller than the uncorrected one. Correspondingly, the hindwing turns upwards the air current directed against the forewing, thereby increasing the angle of attack of the forewing. Thus it is necessary to correct the angles of attack derived from the kinematic analysis.

The correction was calculated from the circulation which corresponded to the lift of the wings at the given time. Thus the component of the circulation along the axis of the hindwing was calculated from the circulation from the forewing at a given moment, and on the basis thereof and with reference to the distance at the given moment between the two wings, the component of velocity created by the circulation from the forewing at right angles to the axis of the hindwing was calculated; this lateral speed, together with the relative speed of the hindwing, produced the correction of the angle of attack. The correction was applied for each wing position; it maximally amounted to 2°.

PHILOSOPHICAL TRANSACTIONS OF THE ROYAL SOCIETY B BIOLOGICAL SCIENCES

(d) Final calculation of force and energy

The thorax must produce a torque about the fulcrum which counteracts the aerodynamic torque and the torque caused by the angular acceleration of the wing masses. Concerning the aerodynamic torque the aerodynamic force **P** acting upon the wing at a given instant was known from its components in the animal's co-ordinate system. Moreover, the corresponding axis of the wing **l** was known from a similar set of components. The component of **P** in the direction of **l** did not produce any torque about the fulcrum and should therefore be subtracted. It was calculated from the scalar product **lP**. Subtracting the components parallel to X, Y and Z from the corresponding components of **P**, the force components required were found from the components of **P** perpendicular to **l** ($P_\perp$).

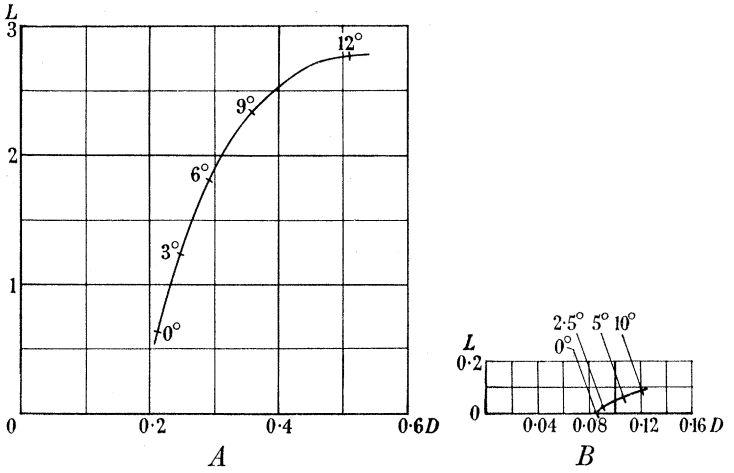

FIGURE III, 15. *A*, polar curve for a locust in position of flight with the wings stretched out in horizontal position. *B*, drag and lift of a locust in position of flight, but without wings. Abscissa and ordinate are drag and lift in grams at a dynamic pressure of 0·1 cm water column.

The point of attack of the aerodynamic force was calculated from the three (forewings) or two (hindwings) weight figures the sum of which was used in calculating **P**. In this way was found the torque Q_a which counterbalanced the aerodynamic torque about the fulcrum.

The movements in figure III, 5 of the wing tip in the $\Phi\Gamma$ co-ordinate system are nearly true to scale, so that the angular velocity can be found graphically (hodograph in figure III, 5). From this the angular acceleration $\dot{\omega}$ was calculated. The torque Q_i necessary to counterbalance the forces due to the acceleration of the wing mass was calculated from $\dot{\omega}$ and from the moment of inertia of the mass (see part VI).

At any instant the thorax must produce a torque equal to the sum $Q_a + Q_i$ representing the magnitude of the extra thoracic wing torque. The angular movements being known, the energy necessary to move the wings could be integrated during any phase of the stroke. This energy does not correspond directly to the work done by the muscles during the same interval of time because of the elastic properties of the thorax (see later papers).

(e) Numerical example

(See Appendix 2)

(*f*) *Extra-to-wing drag*

The aerodynamic effect of the body during flight was measured in an apparatus similar to that used for determining the forces on the wings. A locust without wings and with the legs fixed in the flying position was mounted on the end of the steel bar and in the free current of the wind tunnel (i.e. outside of the boundary layer). The results of the measurements are given in figure III, 15*B*. It will be seen that the resistance of the body varies only slightly in relation to the pitch within the range corresponding to that of the flying animal's (from 5 to 10°) and that the lift is small. However, in the apparatus used for flight experiments, in addition to the drag from the body the animal must also overcome the drag from the suspending bar *P*, figure III, 1. This resistance in grams was measured as 0·052 p_v, p_v being the dynamic pressure in mm of water.

7. Results

The four experiments analyzed (I to IV) all represented flapping flight. In present-day insects this is the basic type of aerial locomotion and the entire construction of the pterothorax is highly influenced by it. However, it is reasonable to consider some possibilities for gliding, since recent investigations on locust swarms have indicated its importance in connexion with thermal up-currents (Rainey & Waloff 1951).

(*a*) *Gliding*

The curve in figure III, 15*A* shows the lift and drag of a *total* standard locust (2 g) with the legs in complete flight attitude and with all wings horizontal and fully extended. The units along both axes are grams per mm water column of dynamic pressure. The relationship represents the *best* gliding possibilities in the desert locust; the gliding ratio for instance corresponds to 1/6·5 at an air speed of 3·8 m/s. Under these conditions soaring should be possible if the speed of the up-current exceeds 0·6 m/s, i.e. at a fairly low degree of thermal convection. In nature the desert locusts seem to glide or soar with the hindwings partially folded (Waloff, personal communication).

(*b*) *Checking the analysis of flapping flight*

The analysis provided detailed information on the variation with time of the aerodynamic forces acting upon the flapping wings. If the basic assumptions are correct the summation during one wing stroke of all vertical components should result in a *calculated average lift* equal to the lift *measured* when the film was taken, i.e. which was determined directly and independently of the proceeding analysis. Similarly, the *calculated average thrust* should be equal and opposite to the *extra-to-wing drag* which was also measured independently. This should provide an overall check on the validity of the calculation.

Average lift

Of the four experiments examined nos. I and II correspond to normal, horizontal flight, the average measured lift being 97 and 111 % of the basic weight respectively. The flying speed was also normal at about 3·5 m/s. The lift in no. III, on the other hand, was very high (162 %), in spite of the lower speed of 3·2 m/s. The last experiment (IV)

PHILOSOPHICAL TRANSACTIONS OF THE ROYAL SOCIETY B BIOLOGICAL SCIENCES

was abnormal in that the measured lift was only 70%, the speed was 3·2 m/s and, in contrast to the other experiments, the legs were not held in flight attitude. The results are given in table III, 3, together with the calculated lift. It appears that the measured and the calculated values correspond very well in the three 'good' experiments (differences −3, 7 and −5%). A crude calculation of the probable error of the analysis indicated 10% as the maximum limit which is consistent with the above result. However, experiment IV deviated too much since the measured lift was only 1·68 g against 2·00 g calculated. In part IV, Weis-Fogh found that the adoption of complete flight posture seemed to be correlated with positive or zero lift during the *upstroke*. It must be remembered that during the first rapid part of the upstroke the wind forces could not be determined with the same accuracy as during the remaining part of the stroke. It is therefore reasonable to suggest that the large discrepancy of 19% between the measured and calculated lifts in no. IV was due to this circumstance (cf figure III, 17). The two lower lines in table III, 3 show that in experiments I to III the hindwings produced three-fourths of the total lift (about two-thirds in no. IV).

TABLE III, 3. THE MEASURED AND THE CALCULATED LIFT

flight no. ...	I	II	III	IV
relative lift (%)	97	111	162	70
animal	♀ *a*	♂ *b*	♂ *c*	♀ *a*
flying speed (m s^{-1})	3·5	3·6	3·2	3·2
lift calculated from analysis of forces (g)	2·17	2·43	2·59	2·00
directly measured lift (g)	2·23	2·26	2·74	1·68
error in lift (g)	−0·06	+0·17	−0·15	+0·32
relative error in lift (%)	−3	+7	−5	+19
lift from forewings (g)	0·66	0·66	0·61	0·65
lift from hindwings (g)	1·51	1·77	1·98	1·35

Average thrust

The average thrust produced by the wings should equal the *extra-to-wing drag* of the locust plus the drag of the suspending bar. The drag of the locust's body was measured with the same apparatus as was used for the determination of the lift and drag of the wings. But the body (complete flight attitude, wings removed) was now placed in the free air current and thus outside the boundary layer. The curve in figure III, 15*B* shows the lift and drag of the body set at different angles to the wind (=different body angles). Along both axes the units are grams per mm water column of dynamic pressure. The two curves in figure III, 15 were drawn to the same scale; it is obvious that the lift of the body is completely insignificant compared with the lift produced by the wings. In bees and other insects Hocking (1953) has claimed that the body could contribute considerably to the lift, but this is certainly not so in locusts.

In addition to the extra-to-wing drag the suspended locust also overcame the drag of the suspension bar. This drag contribution was found to be p_v0·052 g, where p_v was the dynamic pressure in mm water column.

In accordance with table III, 3, table III, 4 shows how the *calculated* thrust corresponded to the *measured* thrust. Again the conformity between the results in experiments I to III was good whereas the calculated thrust was too big in no. IV. It should be remem-

bered that in absolute values the thrust was about fifteen times smaller than the lift, and the accuracy is in fact likely to be smaller than indicated by the discrepancies between the calculated and the measured values. The hindwings produced about three-fourths of the total thrust, apart from experiment IV, which gave a completely aberrant result.

TABLE III, 4. THE MEASURED AND THE CALCULATED THRUST

flight no. ...	I	II	III	IV
relative lift (%)	97	111	162	70
animal	♀ *a*	♂ *b*	♂ *c*	♀ *a*
flying speed ($m\ s^{-1}$)	3·5	3·6	3·2	3·2
thrust calculated from analysis of forces (g)	0·14	0·16	0·11	0·16
resistance of suspension bar (g)	0·040	0·041	0·034	0·034
resistance of body calculated from analysis of forces (g)	0·10	0·12	0·08	0·13
resistance of body direct from flying speed (g)	0·096	0·096	0·082	0·082
error in thrust (g)	0·00	0·02	0·00	0·05
thrust from forewings (g)	0·03	0·04	0·03	0·32
thrust from hindwings (g)	0·11	0·12	0·08	−0·16

Conclusions

The differences between the calculated values and the measured average lift and thrust were not systematic. Moreover, in the three 'good' experiments (nos. I to III) they did not exceed the probable errors of estimation. Experiment IV deviated much from a normal performance (table III, 2, p. 514), and in this case the measured and calculated lifts differed by 19 %. This discrepancy might be due to the difficulty in estimating the wind forces during the rapid part of the upstroke. In general, the deviations do not indicate the presence of any systematic errors. The good conformity between the measured and the calculated forces therefore makes it probable that the principles of steady-state aerodynamics can be applied to locust flight. This is the general background for the detailed treatment of the result.

(*c*) *Changes in lift during a stroke*

In what follows the *lift* means the instantaneous vertical force with which the wings act upon the body. It is positive when opposite to the pull of gravity. The changes in lift during one wing stroke are seen in figures III, 16 to III, 18, where the abscissa is the time since the forewings started to move downwards, T being the duration of one wing stroke. The ordinate shows the lift. Experiments I and II were so near to an average, horizontal flight performance (cf. tables III, 1 and III, 2) that they could be considered as representative for normal flight. The curves in figure III, 16 thus show the normal variation of the lift. The found values are shown as filled circles (I) and crosses (II) respectively, and the curves were drawn as accurately as possible, taking all points into consideration. The lift is expressed as fractions of the average lift produced by both pairs of wings. It is seen that the conformity between the performances of the two individuals is as good as could be expected from the accuracy of the analytical method.

The two forewings (upper curve in figure III, 16) produced positive lift during most parts of the stroke, and it only became zero or slightly negative during the middle part of the upstroke. But the main contribution was due to the middle and later part of the

downstroke where it amounted to about half the body weight. This phase was characterized by maximum angular velocity and, having passed the horizontal position, by the bending down of the rear flap indicated in figure III, 8 (points 9 to 12). The lift produced by the two hindwings (lower curve) followed the same general course, but the maximum was more distinct and coincided with the horizontal wing position, i.e. with the maximum angular velocity. The maximum lift of the hindwings amounted to one and a half times the body weight. When integrated over the total stroke, the hindwings produced 71 % of the lift. The share of lift produced during the upstroke was 14 % in the hindwings and only 6 or 7 % in the forewings, i.e. about 20 % in all. In both pairs of wings the variation of lift with time was rather complicated and did not correspond to a simple sine function. It should be noted that the lift never became negative.

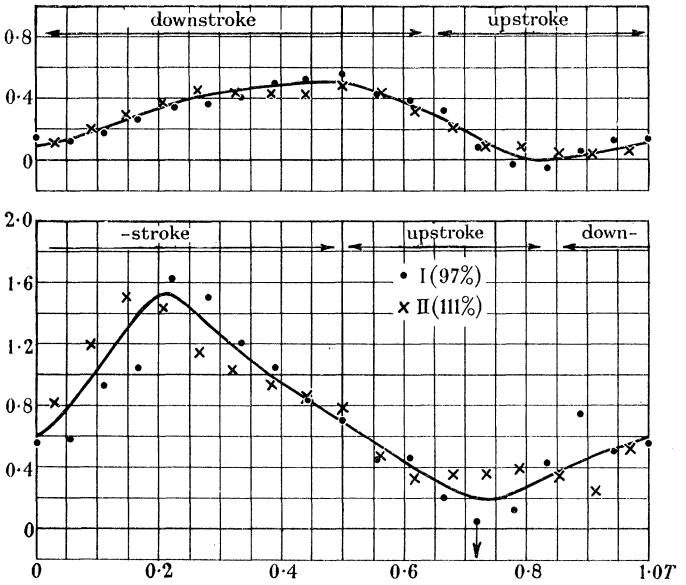

FIGURE III, 16. Lift of the wings during a wing stroke. Top, for the two forewings; below, for the two hindwings. Abscissa: time during a wing stroke beginning at the top position of the forewing. Ordinate: lift in relation to the average lift of all four wings. The curves represent normal flight. It should be noted that the variation of the lift with the time is by no means sinusoidal.

The results from the other two experiments are seen in figure III, 17. The units *and* the curves are the same as in figure III, 16. It is seen that the general course of variation was the same as during normal flight both when the lift was high (162 %, crosses) and when it was low (70 %, open circles). If we express the instantaneous lift as a fraction of the average lift L produced in each experiment, the maximum relative lift during the middle part of the downstroke is seen in table III, 5. The conformity between these results justifies the procedure used by Weis-Fogh (part IV) to estimate the angles of attack during the downstroke from more easily measurable flight parameters. Figure III, 18 shows the lift in experiments I and II when the contributions from forewings and hindwings were summed. The axes are similar to those in figure III, 16. The lift is seen to oscillate about 100 % ($1{\cdot}0\bar{L}$) in a nearly saw-tooth curve. Thus the differences in phase between the two pairs of wings and the different duration of upstroke and downstroke

are no longer detectable, giving rise to the rather simple, broken curve of the calculated *changes* in vertical speed and displacements of the freely flying locust (see discussion on p. 546).

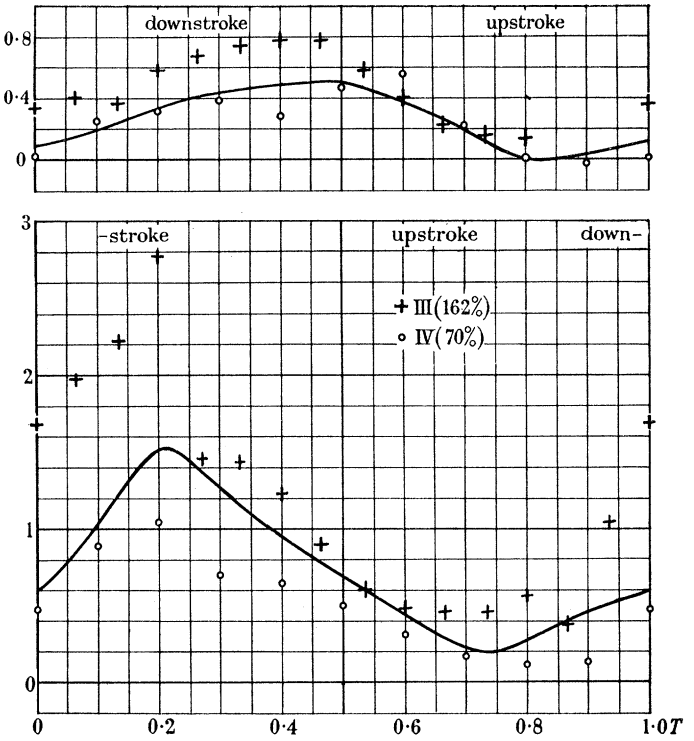

FIGURE III, 17. Lift of the wings during a wing stroke. Abscissa and ordinate as in figure III, 16. The curves represent normal flight. The points are derived from experiment III with a special high lift (crosses) and experiment IV with a special low lift (circles). No. IV is problematical.

TABLE III, 5. THE LIFT PRODUCED DURING MIDDLE PART OF DOWNSTROKE AS A FRACTION OF THE AVERAGE LIFT

no.	forewings	hindwings	sum
I+II	0·5	1·4	1·9
III	0·5	1·4	1·9
IV	0·6	1·4	2·0

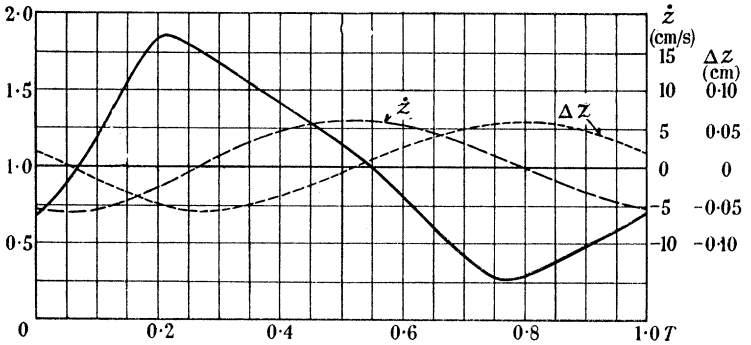

FIGURE III, 18. Vertical forces and movements during normal flight. The lift from all four wings is shown by the full line. Abscissa and ordinate (left) as in figure III, 16. The freely flying animal's vertical speed caused by varying lift (ordinate to the right) is represented by the broken curve. The curve Δz represents the freely flying animal's vertical displacements during a wing stroke (ordinates at the extreme right).

In Osborne's (1951) theory on flapping flight, it was assumed that lift was mainly produced during the downstroke. This is approximately true in the desert locust when the two pairs of wings were considered separately, but the phase differences and the relatively large lift of the forewing (flap mechanism) during the latter half of the downstroke both tend to obscure this effect when the curves are summed. While it was reasonable to test Osborne's theory as far as the average force coefficient was concerned (part I), the summated *variations* in lift experienced by the body bears no relation to that deduced from any existing theory.

(*d*) *Changes in thrust during a stroke*

The thrust means the instantaneous force with which the wings act upon the thorax parallel to the axis; it is positive in the direction of flight. During normal flight (experiments I and II) the thrust varied as seen in figure III, 19. The time axis starts when the forewings begin to move downwards; the ordinate is the thrust in fractions of the total average thrust produced by both pairs of wings. The upper curve derives from both forewings, the middle curve from both hindwings, and the lower curve is the sum of the two.

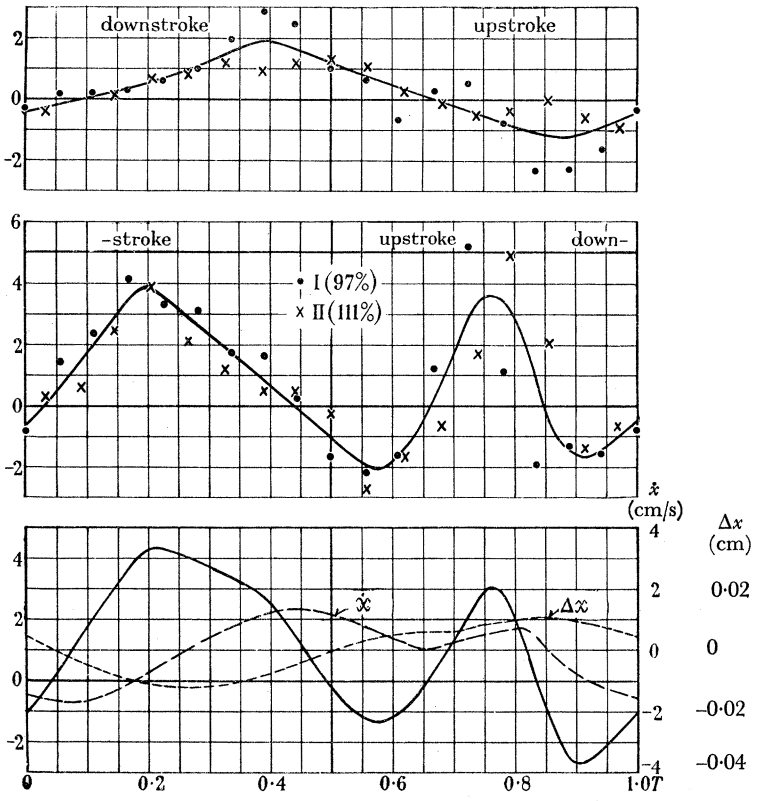

FIGURE III, 19. Thrust during a wing stroke. Abscissa: the time during a wing stroke from top position of the forewing. Ordinate: thrust in relation to average thrust from all four wings. The curves represent normal flight. Above, the two forewings; in the middle, the two hindwings. It should be noted that the variation of the thrust with time is much more complicated than perhaps it might have been expected. It is, of course, impossible to approximate with a simple function of a sine. In the figure below the full curve shows the thrust from all four wings. The curve $\dot{x}$ represents the additional speeds which a freely flying animal will attain on account of the variation of the thrust. The curve Δx represents the displacements of a freely flying animal either before or behind the positions corresponding to a steady flying speed.

The forewings produce positive thrust only during the downstroke, while it is negative during most of the upstroke. The hindwings, on the other hand, contributed by positive amounts during both phases, while the transition from upstroke to downstroke as well as from downstroke to upstroke give rise to negative thrusts. The summated lower curve therefore became very complicated. It should be noted that the average thrust only amounts to 7 % of the average lift. Maximum of thrust coincides with maximum of lift, the ratio between them being 1/7. It is therefore reasonable to suggest that the complicated variation of the thrust is of only small importance, a suggestion which is further illustrated by the two broken curves showing the small *changes* in horizontal speed and displacement to be expected in a locust in free flight (see discussion on p. 546).

(*e*) *Angle of attack*

Since the angle of attack changes continuously from wing base to wing tip it is not a simple parameter and cannot be described as a simple curve. It is, however, possible to obtain an idea of the variations during a wing stroke when we confine ourselves to the wing section situated midway between base and tip. Figure III, 20 shows how the corresponding angle of attack α_m varied in experiments I (filled circles) and II (crosses). The length of the vertical hatching lines indicates the magnitude of the lift (from figure III, 16). The curves differ very much from the sinusoidal oscillation applied in Holst & Küchemann's theory (1941), but in both pairs of wings they have, in fact, some resemblance with the basic assumption made by Walker (1925). During the downstroke α_m remained nearly constant and averaged 11·6° in the forewings and 14·7° in the hindwings. These figures are worth comment because they make possible a direct test of Osborne's theory of flapping flight discussed in part I. When the average *minimum* coefficients during the downstroke $\sqrt{(\overline{C}_L^{d^2}+\overline{C}_D^{d^2})}$ were calculated for a standard locust in steady horizontal flight at 3·6 m/s the coefficients were 0·55 in the forewings and 0·94 in the hindwings (part I, table I, 7). In experiments I and II the empirically determined values were 0·9 in both pairs of wings. Since the hindwings produced three-fourths of the total lift, and since the various theoretical assumptions could only be approximations to true flight, a better conformity could hardly be expected. Osborne's theory is therefore in fair agreement with the experimental results as far as locusts are concerned.

Another interesting feature was observed. In figure III, 21 the curves from figure III, 20 have been reproduced, but, in addition, the angle of attack α_m is shown both in experiment III (high lift, crosses) and in experiment IV (low lift, open circles). It appears that the high lift was achieved by increasing the angle of attack as compared with normal lift without altering the main features of its variation. In both pairs of wings the angles were near to the stalling limit during the entire downstroke. Since, apart from the wing twisting, all wing-stroke parameters are extremely constant in locusts, and since experiment III took place at a speed of 3·2 m/s which was subnormal it was concluded that the flying speed must be increased above 3·2 m/s if a locust is to lift more than one and a half times its basic weight, as must be the case with pregnant females.

In experiment IV, α_m was both higher and lower than in normal flight. However, this experiment deviated in so many respects from the average that no conclusions could be drawn from it; it was reasonable to conclude that the magnitude of the lift is normally

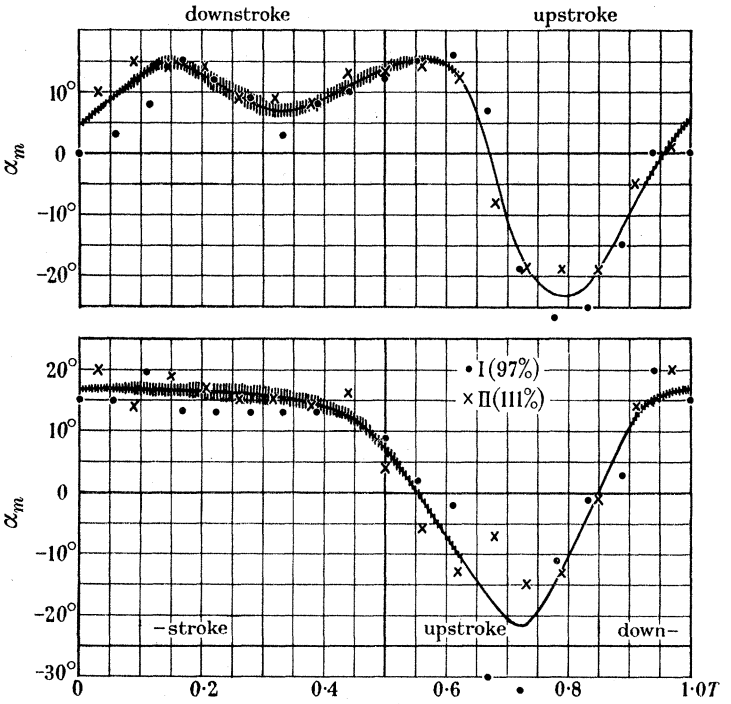

FIGURE III, 20. The angle of attack at the mid-point of the wings. Abscissa: the time during a wing stroke from top position of the forewing. Ordinate: the angle of attack. Above, forewing. Below, hindwing (here the angle of attack is the angle between the foremost, stiff sector of the wing and the air current). The curves correspond to normal flight. The thickness indicates the magnitude of the lift.

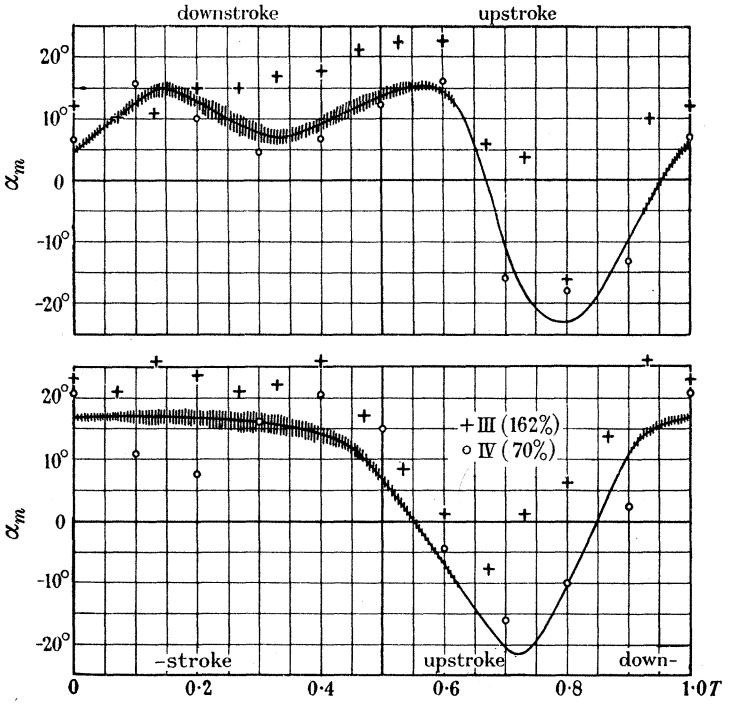

FIGURE III, 21. The angle of attack at the mid-point of the wings. Abscissa and ordinate as in figure III, 20. Above, forewing. Below, hindwing. The curves represent normal flight. The points indicate extraordinarily high lift (+) and an extraordinarily low lift (○). The thickness indicates the magnitude of the lift.

PHILOSOPHICAL TRANSACTIONS OF THE ROYAL SOCIETY B BIOLOGICAL SCIENCES

determined by the angle of attack. This direct evidence strongly supports the indirect evidence given in part II, namely, that the main factor responsible for the adjustment of the lift consists of an adjustment of the wing twisting rather than of any other wing-beat parameter. It is also consistent with the findings in part IV, where it is shown that when the body angle was changed, the lift was kept constant by an active alteration of the wing twisting.

The results do not permit a similar analysis of the factors governing the thrust, but its low numerical value makes such a treatment of little interest in locusts.

(*f*) *Torques about the fulcrum*

In part I, p. 431, we considered the torques about the wing fulcrum. At any instant the sum of the torque contributions must be zero (equation (I, 6)):

$$Q_m + Q_a + Q_i + Q_e + Q_d = 0.$$

Q_m is the torque produced by the flight muscles, Q_a is the aerodynamic torque, Q_i the torque caused by the acceleration of the wing masses or the inertial torque, Q_e is the torque due to the elastic deformations of the thorax, and, finally, Q_d is the torque due to the extramuscular damping inside the thorax.

The present analysis makes it possible to estimate the variation with time of the two extra-thoracic contributions Q_a and Q_i, the sum of which represents the total extra-thoracic torque counterbalanced by the thorax. The corresponding torques $-Q_i$ and $-Q_a$ produced by the thorax in the course of one wing stroke are seen in figures III, 22 and III, 23, where the ordinate is the torque in g cm. The upper parts of these figures show the torques about the X-axis, Q_X; the sense was positive when the torque tended to turn the wing upwards. The lower parts show the torque about the Z-axis, Q_Z, the sense being positive when the torque tended to turn the wing forwards. In figure III, 22 the broken curves show components of $-Q_a$ and $-Q_i$ about the X-axis for the two forewings in experiment I. The full curve is their sum and is equal to the vertical torque which the thorax must produce against the vertical extra-thoracic forces. The aerodynamic torques about the Z-axis were negligible, so that the full curve was identical with the variation of the horizontal component of $-Q_i$. The corresponding curves are seen in figure III, 23 when summed for *the two hindwings*.

It is obvious from the figures that in both pairs of wings the torques varied with time in a very complex way. This is true for the single contributions as well as their sum. Furthermore, the inertial torques are of the same order of magnitude as the aerodynamic torques. Indeed, the mass forces of the wings of *Schistocerca gregaria* gave rise to the numerically largest torques and are also of great importance in the energy account. It is unlikely that a reasonably simple theory can be developed which would make it possible to calculate the course of the broken curves in figures III, 22 and III, 23. Since the energetics of flight can only be understood from the variation with time of the individual torque contributions, figures III, 22 and III, 23 therefore show why a laborious empirical analysis was considered necessary.

It has been found that the elastic torque Q_e in equation (I, 6) (p. 431) is of significant magnitude. It is therefore not possible from the present analysis to estimate accurately the muscular torque Q_m.

PHILOSOPHICAL TRANSACTIONS OF THE ROYAL SOCIETY B BIOLOGICAL SCIENCES

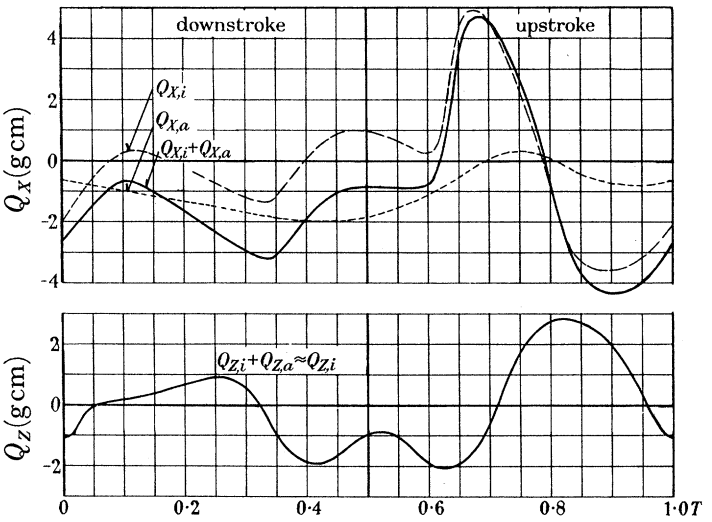

FIGURE III, 22. The torque in the pair of forewings at the base section. Abscissa: time during a wing stroke from top position of the forewing. Ordinate: torque in g cm. Above, the sign is positive for upward turnings of the wing; below, it is positive for forward turnings. Above, the torque about the vertical; the aerodynamic torque is here small so that the lower curve representing the total torque, also with approximation, shows the torque due to acceleration.

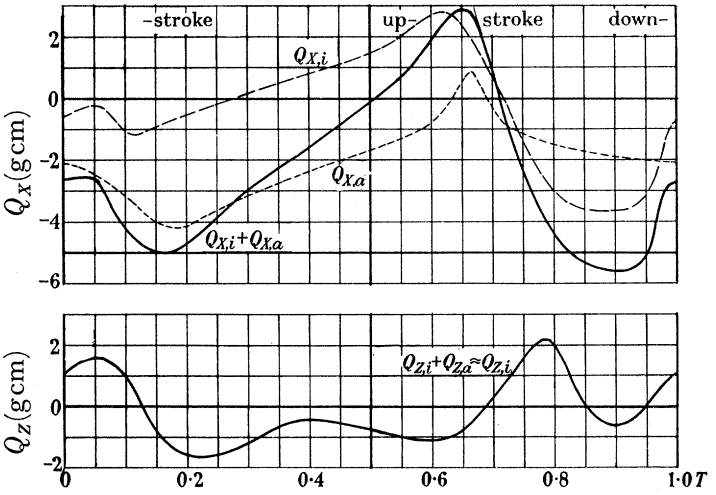

FIGURE III, 23. The torque in the pair of hindwings at the base. Otherwise as in figure III, 22.

(*g*) *Notes on the total power transmitted to the wings*

Although a more complete treatment will be given later, it is instructive to consider the magnitude of the power transmitted to the wings.

Figure III, 24 shows the variation of the total work (aerodynamic+inertial) transmitted through the fulcrum during one wing stroke. The two pairs of wings are considered separately. The total power passing the fulcrum must be related to the total power consumption of the flight muscles P of which the fraction eP is available for mechanical work, e being the mechanical efficiency of the muscle system. It is, however, difficult to estimate eP by summating the aerodynamic power and the inertial power: (1) partly because there are two pairs of wings which might be mechanically coupled, (2) partly because energy may be stored and released in the elastic body cuticle (Q_d seemed to be

insignificant; Weis-Fogh, part VII), and (3) finally because the mechanical efficiency of muscles varies greatly with the working conditions; thus a given numerical amount of work generally demands a considerably smaller energy consumption when the work is negative than when it is positive (Abbott, Bigland & Ritchie 1952; Asmussen 1953). If only the two last phenomena are considered we have

$$eP = P_p + fP_n,$$

where P_p is the positive power, P_n is the negative power, and f is a factor varying from $+1$ to -1.

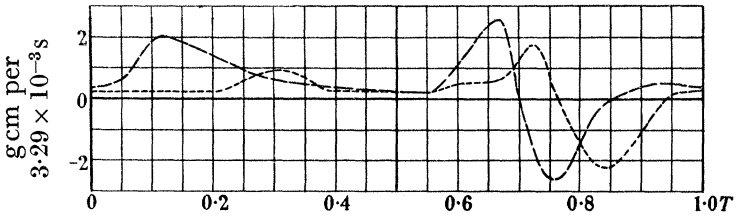

FIGURE III, 24. The variation of the work during the wing stroke. Abscissa: time during a wing stroke from top position of the forewing. Ordinate: work in g cm. The work is positive when the projection of the force on the movement points in the same direction as the movement. The dotted curve represents the work of the two forewings, and the pecked line represents that of the two hindwings.

TABLE III, 6. THE EXTRA-THORACIC POWER OUTPUT FOR DIFFERENT VALUES OF f

flight no. ...	I	III
relative lift (%)	97	162
animal	♀ *a*	♂ *c*
flying speed (m s^{-1})	3·5	3·2
power ($f=-1$) (kcal h^{-1} kg^{-1})	7·1	11·2
($f=0$) (kcal h^{-1} kg^{-1})	12·0	13·7
($f=0{\cdot}2$) (kcal h^{-1} kg^{-1})	13·0	14·6
($f=1$) (kcal h^{-1} kg^{-1})	16·9	16·2

Let us consider the extreme cases. Provided the flight system possessed ideal elastic properties all negative work would be stored and be released during the positive phases. f would then be -1. If, on the other hand, the negative work were completely absorbed by viscous brakes, f would be 0. The third extreme is that all negative work was overcome by the action of muscles which were stretched while being stimulated. f would then be positive but smaller than 1; its magnitude would be given by the ratio between the mechanical efficiencies during positive work (contraction) and negative work (stretching) respectively. This ratio depends upon the speed of deformation; for instance, in human muscles working at medium speeds it ranges about 0·2 (Asmussen 1953).

Provided then that the two pairs of wings were worked by completely independent muscle systems, the extra-thoracic work done per stroke could be calculated for each pair of wings in figure III, 24. Table III, 6 summarizes the total extra-thoracic power outputs in experiments I and III when f was given the values -1, 0, $+0{\cdot}2$ and $+1$ in turn. These results show that a detailed knowledge is necessary of the mechanical properties of the pterothorax in order to understand the energetics of flight. The magnitude of the

power output (10 to 15 kcal kg^{-1} h^{-1}) was about ten to five times less than the total energy conversion during flight (*ca.* 70 kcal kg^{-1} h^{-1}; Weis-Fogh, part VIII). However, a more detailed discussion of the energetics will be given in part IX (Martin Jensen & Weis-Fogh).

8. Discussion

(*a*) *Errors caused by restriction of freedom*

During the experiment the locust was fixed to a rigid suspending bar. In free flight the rapid changes in lift and thrust demonstrated in the previous chapter would cause the locust to oscillate up and down along the Z-axis and to and fro along the X-axis. The changes in force might also produce rhythmical oscillations of the body angle, i.e. of the angle between the long body axis and the horizontal wind. The analytical method was not accurate enough to make possible a calculation of the moments of the resulting forces about the centre of gravity. It was therefore not possible to estimate to what extent the body angle was likely to oscillate in free flight. In part II it was found that freedom to pitch did not seem to influence the performance significantly compared with experiments where the body angle was fixed at the same average value. The translatory movements along the Z- and X-axes could, however, be estimated fairly accurately.

Vertical movements

It appears from figure III, 18 that the locust lifted more than its body weight from $0{\cdot}06T$ to $0{\cdot}55T$. Consequently it would have been accelerated upwards if not fixed to the suspending bar. The opposite is true during the remaining part of the wing stroke. The maximum lift was 1·86 times the body weight, and at that instant the suspending must have acted upon the sternum with a force corresponding to 0·86 time the weight.

The vertical velocity $\dot{z}$ of the freely flying locust could be estimated by integrating the areas between the full curve and the line denoting mean lift in figure III, 18. A second integration gave the displacement Δz from the mean altitude which the centre of gravity would undergo during one wing stroke. The ordinate units for $\dot{z}$ and Δz are seen at the right-hand side of the graph. The maximum vertical velocity was only 6 cm/s, and the maximum displacement was less than 1 mm, i.e. they were both of insignificant order of magnitude.

Horizontal movements

In a similar way figure III, 19 served as a basis for calculating the changes in horizontal velocity $\dot{x}$ and the corresponding changes in horizontal displacement Δx above and below the mean velocity of 350 cm/s. The largest additional velocity was 2 cm/s and the largest additional displacement was only 0·1 mm.

Conclusion

The rhythmic changes in lift and thrust were such that the corresponding rhythmic *changes* in translational velocity and displacements which would occur during free flight were insignificant compared with the *average* velocities and displacements. It is therefore

reasonable to conclude that the main results from the present analysis of suspended flight will also be representative for free horizontal flight provided that steady-state aerodynamics can be applied to flapping flight.

(*b*) *Errors caused by non-stationary air flow*

The results strongly indicate that the flapping flight of locusts can be treated as a sequence of steady-state flow situations. This, also, is the assumption made in most theories on flapping flight hitherto published. It is therefore reasonable to discuss the probable limits of this assumption.

Reynolds's number

In *Schistocerca gregaria Re* is of order of magnitude of 2000. The general application of the polar diagrams in figures III, 12 to III, 15 is therefore not only restricted to a graduated wind field (figure III, 11) but strictly speaking also to flow situations with the same value of *Re*. However, the general form of the curves can possibly be considered typical for the long rigid wing type (forewings, figures III, 12 and III, 13) and for the broad flexible wing type (hindwings, figure III, 14), both of which are common in flying animals.

In many small insects *Re* may drop to a few hundreds (Holst & Küchemann 1941). The resistance coefficient of spheres, disks, cylinders, etc., are fairly constant from $Re = 10^5$ to 10^3 but generally start to increase when *Re* is further lowered. Concerning airfoils we are ignorant of the effect of low values of Reynolds's number upon the coefficients of lift and drag. We are also ignorant of the time necessary to build up a circulation corresponding to the lift produced in a steady-state flow. In these experiments *Re* was the same during flight as it was when the lift/drag relationship was measured so that only the last uncertainty remains. The following considerations indicate that this time factor is of little quantitative importance in locust flight. This might not be so in small insects with a high wing-beat frequency, but the problem ought to be studied experimentally.

Change in circulation

The principle of flapping flight implies that the lift produced by a wing must change rhythmically during the stroke. In order to estimate the importance of the non-steady phases Holst & Küchemann (1941) suggested the use of the frequency parameter

$$\nu = \frac{nl}{v},$$

where n is the true frequency, l is the length of the wing, and v is the flying speed (see Küssner 1936; Küssner & Schwarz 1940). ν has proved useful as a basic parameter in the case of vibrations of aeroplane wings and wind-induced oscillations of suspension bridges. However, since the stroke angle does not enter the expression, it is unlikely that it can express the extent to which flapping flight is based upon stationary flow. Consider two flight performances the kinematics of which are similar apart from the stroke angle which is much bigger in the one case than in the other. ν would then be the same in both. But it is evident that the performance in which the stroke angle is small could with better approximation be regarded as a sequence of stationary flows than could the other.

A better basic parameter seems to be the figure k used by Walker (1925, 1927); k is the

ratio between the vertical speed of a characteristic point of the wing and the horizontal speed ($\approx$flying speed)

$$k = \frac{2n\phi}{v} r,$$

where n is the frequency, ϕ is the stroke angle, v is the forward speed, and r is the distance from the fulcrum to the point considered. k is of course not defined for hovering flight where $v = 0$. A further discussion concerning v and k is found in part I (p. 440).

In this context another type of approach is suggested. Since it only concerns the dimensions of some fundamental feature of flapping flight a considerable simplification is justified. The S-shaped line in figure III, 25 shows the course of a cross-section of the wing through the air during a downstroke. This section represents the total wing and was therefore chosen at distance r from the fulcrum, where r is the radius of inertia of the wing area (about fulcrum). It is assumed that the wing is moved with a constant air speed V during the downstroke and that the lift is only produced during the downstroke while it is zero during the upstroke. In the upper position u, the wing will therefore have no circulation.

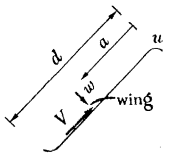

FIGURE III, 25.

When the wing leaves u a starting vortex is formed which is left at u and whose strength Γ depends upon the lift. At any point of the downstroke in the distance a from u, this starting vortex induces a cross-wind w at the wing, where

$$w = \frac{\Gamma}{2\pi a}.$$

As long as w is of significant magnitude compared with V the wing is still in its non-stationary phase. But when the ratio w/V is small, the flow can be considered as stationary. We now assume that the ratio is small in the distance a from u, giving

$$\frac{w}{V} = \epsilon_1 = \frac{\Gamma}{2\pi a V}.$$

If the total stroke is to be analysed from stationary situations, it is a requirement that the initial situation only comprises a small part of the total downstroke d, i.e. $a/d = \epsilon_2$. The condition for a stationary analysis then is that $\epsilon_1 \epsilon_2$ should be small or $2\pi\epsilon_1\epsilon_2 = \Gamma/(Vd) =$ small. If the lift is L and the length of the wing l we have $\Gamma = L/(l\rho V)$, from which we get the dimensionless expression

$$2\pi\epsilon_1\epsilon_2 = \frac{L}{l\rho V^2 d}.$$

With the accuracy of measurement applied in the present investigation it was reasonable to allow ϵ_1 and ϵ_2 to attain the value 0·1. The condition for performing a stationary analysis then becomes $L/(l\rho V^2 d) = 0{\cdot}06$.

In the forewings of *Schistocerca* the figures work out as 0·02 and in the hindwings 0·05

In spite of the oversimplifications (*inter alia* no lift at the start of the downstroke), this estimate indicates that the present analysis of locust flight cannot be performed more

accurately if non-stationary flow situations are taken into account. Within the degree of accuracy, the flow should be stationary provided that the time factor in establishing the circulations can be disregarded. The conformity between the calculated and the measured forces indicates that this is the case.

(*c*) *Notes on stationary flow in other insects*

A more general question arises: can the flight of other insects also be regarded as the result of a sequence of stationary flow situations. From a critical discussion and recalculation in part I of some of Osborne's results (1951), it was concluded that 'there is little to be said against and much in favour of considering natural flight as being based upon conventional aerodynamic principles, even in case of small insects like mosquitoes' (p. 416). *Inter alia* this conclusion was based upon calculations of the minimum force coefficients of a flying 'horse-fly type' and of a 'mosquito type', the details being given in figure I, 8 and in table I, 7 in part I. It was assumed that lift was only produced during the downstroke, but the calculations did not take the influence of the starting vortex into account. This might have been a serious omission because the starting vortex tends to diminish the lift at the beginning so that much higher lift coefficients would be necessary during the following phases than would be ascertained from the estimate of the mean taken over the entire downstroke. In the small insects described in part I (table I, 1), $2\pi\epsilon_1\epsilon_2$ amounted to 0·07 both in the 'horse-fly type' and in the 'mosquito type'. The wing-stroke frequency of the small insects was therefore adjusted to the size of the animals in such a way that the starting vortex would not diminish the average lift to any bigger extent than was the case in locusts. The desert locust weighed about 600 times more than the mosquito.

In the dimensionless expression $L/(l\rho V^2 d)$, V was the true air speed of the wing section. It depends upon both the flying speed and the flapping speed. In many insects the flying speed varies between 2 and 4 m/s and the flapping speed is generally the biggest. The latter is directly proportional to the wing-stroke frequency and to the stroke angle. Since the stroke angle is also of the same magnitude in insects of different sizes (1·5 to 2 rad), it follows that $n \propto l^{-1}$ in insects with the same ratio between non-stationary and stationary flow. This type of relationship has been deduced from a number of quite different dimensional considerations (part I, p. 436).

I am greatly indebted to the late Professor August Krogh, For.Mem.R.S.; I furthermore thank Mr N. Franck, civil engineer, for his able assistance and Dr J. W. S. Pringle, F.R.S., for his comments upon the MS. The Scandinavian Insulin Foundation, Copenhagen, has supported the work.

Appendix 1

Numerical example of the kinematic calculations

As an example of the numerical treatment, the calculation for a single point will be shown here. The point chosen is no. 5, which for the forewing is at the beginning of the downstroke and for the hindwing is just in the middle of the downstroke.

Measurements from the photograph give for the tip of the forewing $X = -1{\cdot}96$ and $Z = 3{\cdot}31$ cm, and since the true length from the fulcrum to the indicator point on the wing tip is 6·39 cm, Y is calculated to be 5·10 cm. The values must be corrected for the distor-

tion of the perspective. The distance from the objective to the ZX-plane is 27·0 cm, the distance to the wing tip is $27{\cdot}0-5{\cdot}10=21{\cdot}9$ cm, and the scale for the measurements on the photograph refer to a distance of 23·5 cm; therefore the measured values of X and Z must be corrected by multiplication by 21·9/23·5. The true co-ordinates are now $X=-1{\cdot}83$ cm, $Z=3{\cdot}09$ cm, and $Y=5{\cdot}29$ cm.

On picture no. 4, the corrected co-ordinates XYZ to the wing tip are $-1{\cdot}94$, 5·03 and 3·43 cm, and on picture no. 6 they are $-1{\cdot}13$, 5·71 and 2·64 cm.

The average displacement in the direction of X is $\frac{1}{2}(-1{\cdot}13+1{\cdot}94)=0{\cdot}40$ cm, and the displacements in the directions of Y and Z are 0·34 and $-0{\cdot}40$ cm respectively, all corresponding to the time interval between the pictures.

The flying speed was 350 cm/s, the wing frequency 17·50 s^{-1} and the number of pictures per wing stroke 17·4. Between two pictures, the animal moved $\frac{350}{17{\cdot}50\times 17{\cdot}4}=1{\cdot}15$ cm in the direction of x in the co-ordinate system of the flight. In this system, the movement of the wing tip per picture is $x=0{\cdot}40+1{\cdot}15=1{\cdot}55$ cm, $y=0{\cdot}34$ cm and $z=-0{\cdot}40$ cm, and the velocity is obtained by multiplication by the wing-stroke frequency and the number of pictures per stroke $\mathbf{v}=471\ \ 103\ \ -122$ cm/s. The numerical value of the velocity is $v=497$ cm/s.

The longitudinal axis of the wing is: $\mathbf{l}=-1{\cdot}83\ \ 5{\cdot}29\ \ 3{\cdot}09$ cm. The scalar product of this vector and $\mathbf{v}$ is $-1{\cdot}83\times 471+5{\cdot}29\times 103+3{\cdot}09\ (-122)=-694$. The numerical value of the two vectors being 497 and 6·39, the pitch of the wing in relation to the direction of the air current is

$$\beta=\text{arc cos}\ \frac{-694}{497\times 6{\cdot}39}=103°.$$

The treatment of the cross-line c_t at the wing tip is shown in figure III, 7, and the co-ordinates to the cross-line are $\mathbf{c}_t=0{\cdot}955\ \ 0{\cdot}276\ \ 0{\cdot}104$, $c_t=1{\cdot}000$. The normal to the plane determined by $\mathbf{v}$ and $\mathbf{l}$ will be $\mathbf{n}=961\ \ -1231\ 2684$, $n=3110$. The angle between $\mathbf{n}$ and $\mathbf{c}_t$ is $\frac{1}{2}\pi-\alpha$, α being the angle of attack which may be calculated from

$$\cos\ (\tfrac{1}{2}\pi-\alpha)=\frac{961\times 0{\cdot}995-1231\times 0{\cdot}276+2684\times 0{\cdot}104}{3110\times 1{\cdot}000}=0{\cdot}284,\ \alpha=16°.$$

A corresponding calculation of the velocity in the co-ordinate system of flight, the turn of the longitudinal axis in relation to the air current and the angle of attack is also carried out for the mid-point of the longitudinal axis of the wing. The results obtained are $v=419$ cm/s, $\beta=105°$, $\alpha=7°$.

At the wing base $v=350$ cm/s, $\beta=107°$, $\alpha=5°$.

At the point 5 the co-ordinates to the foremost indicator point on the hindwing are $\mathbf{l}_1=-1{\cdot}70\ \ 5{\cdot}56\ \ 0{\cdot}25$ cm, $l_1=5{\cdot}83$ cm.

The velocity of the point is calculated from the position in the preceeding picture and the following one in the co-ordinate system of flight: $\mathbf{v}=593\ \ 73\ \ -331$ cm/s, $v=683$ cm/s. From $\mathbf{l}_1$ and $\mathbf{v}$ is calculated $\cos\beta=-0{\cdot}13$, $\beta=98°$.

The normal to the plane determined by $\mathbf{v}$ and $\mathbf{l}_1$ is $\mathbf{n}=1860\ \ 710\ \ 3430$, $n=3970$.

The vector from the fulcrum to the hindmost indicator point is $\mathbf{l}_2=-2{\cdot}10\ \ 4{\cdot}93\ \ -0{\cdot}10$ cm, $l_2=5{\cdot}36$ cm. The normal to the plane determined by $\mathbf{l}_1$ and $\mathbf{l}_2$ is $\mathbf{m}=0{\cdot}68\ \ 0{\cdot}35\ \ 3{\cdot}33$, $m=3{\cdot}42$. The angle of attack is the scalar product of the normals of the two plans, $\alpha=18°$.

At the base of the hindwing $v=350$ cm/s, $\beta=107°$, $\alpha=5°$.

PHILOSOPHICAL TRANSACTIONS OF THE ROYAL SOCIETY B BIOLOGICAL SCIENCES

Appendix 2

Numerical example: wind forces, torque and power

Wind forces

$\alpha_t = 17°$ (corrected due to circulation from hindwing), $\beta_t = 103°$ and $v_t = 497$ cm/s. The polar curves in figure III, 12 give $C_L = 1{\cdot}03$ and $C_D = 0{\cdot}170$. The dynamic pressure is $0{\cdot}154$ g cm^{-2}. The surface area of the wing is $6{\cdot}04$ cm^2. The forces on the wing are $L = 0{\cdot}958$ g and $D = 0{\cdot}158$ g.

The normal to the plane containing **l** and $\mathbf{v}_t$ in the animal's co-ordinate system is $\mathbf{n} = 961 \quad -1231 \; 2684$ with the numerical value $n = 3110$. The components of L parallel to the axes of the animal's co-ordinate system $\mathbf{L} = 0{\cdot}296 \quad -0{\cdot}380 \quad 0{\cdot}829$.

The opposite vector of the velocity has the co-ordinates $-\mathbf{v}_t = -471 \quad -103 \quad 122$, $v = 497$ cm/s. $\mathbf{D} = -0{\cdot}150 \quad -0{\cdot}033 \quad 0{\cdot}039$ g, $\mathbf{P}_t = 0{\cdot}146 \quad -0{\cdot}413 \quad 0{\cdot}868$ g.

At the mid-point of the wing $\alpha_m = 8°$, $\beta_m = 105°$ and $v_m = 419$ cm/s. A corresponding calculation gives $\mathbf{P}_m = 0{\cdot}059 \quad -0{\cdot}270 \quad 0{\cdot}523$ g.

At the wing base, $\alpha_b = 6°$, $\beta_b = 107°$ and $v_b = 350$ cm/s. $\mathbf{P}_b = -0{\cdot}023 \quad -0{\cdot}148 \quad 0{\cdot}253$ g.

Then the wing forces are calculated as the mean values of $\mathbf{P}_t$, $\mathbf{P}_m$ and $\mathbf{P}_b$ with the respective weights 0·18, 0·50 and 0·32.

$\mathbf{P} = 0{\cdot}048 \quad -0{\cdot}260 \; 0{\cdot}499$, $P = 0{\cdot}57$ g.

Torque and power

At point 5 the axis of the forewing was calculated to $\mathbf{l} = -1{\cdot}83 \quad 5{\cdot}29 \quad 3{\cdot}09$ cm, $l = 6{\cdot}39$ cm. At the same moment of time, the aerodynamic force on the forewing was $\mathbf{P} = 0{\cdot}048 \quad -0{\cdot}260 \quad 0{\cdot}499$ g, $P = 0{\cdot}57$ g. $\mathbf{l}.\mathbf{P}/l = 0{\cdot}017$. The co-ordination of **P**'s component parallel to **l** will then be $-0{\cdot}005 \quad 0{\cdot}014 \quad 0{\cdot}008$, the co-ordinates of **P**'s component perpendicular to **l** will be $\mathbf{P}_\perp = 0{\cdot}054 \quad -0{\cdot}274 \quad 0{\cdot}491$ g. $\mathbf{P}_\perp$ is situated in a plane normal to the wing and it may be resolved into a component in the direction of flight and a component perpendicular to the latter:

$$P_x = 0{\cdot}054 \text{ g} \quad \text{and} \quad P_{yz} = \sqrt{\{(-0{\cdot}274)^2 + 0{\cdot}491^2\}} = 0{\cdot}564 \text{ g}.$$

The conditions for this resolution correspond to the development to correct scale in the co-ordinate system.

P is the result of adding $\mathbf{P}_t$, $\mathbf{P}_m$ and $\mathbf{P}_b$ with respect to the weights 0·18, 0·50 and 0·32. The distance l' of the point of attack from the wing base is thus obtained from $Pl' = 0{\cdot}18P_t l + 0{\cdot}50P_m \tfrac{1}{2}l + 0{\cdot}32P_b 0. \quad 0{\cdot}57l' = l(0{\cdot}18 \times 0{\cdot}868 + 0{\cdot}25 \times 0{\cdot}523)$, $l' = 3{\cdot}19$ cm. The torque about the wing base will have a component of $0{\cdot}54 \times 3{\cdot}19 = 0{\cdot}17$ g cm turning forward, and thus the thorax must produce a forward-turning torque of $-0{\cdot}17$ g cm. In the animal's cross-plane the aerodynamic forces will produce a torque of $0{\cdot}564 \times 3{\cdot}19 = 1{\cdot}80$ g cm turning the wing upward, and consequently the thorax must turn the wing with a torque of $-1{\cdot}80$ g cm upward.

At the instant under consideration, the angular velocity of the forewing has a forward and downward direction. From the velocity curve in figure III, 5, there may be calculated an angular acceleration in forward direction of 3600 s^{-2} to the point and a crosswise angular acceleration (positive, corresponding to an upstroke) of -1800 s^{-2}. The moment of inertia of the wing's mass is $2{\cdot}81 \times 10^{-8} \times 6{\cdot}04^5 = 0{\cdot}226 \times 10^{-3}$ g cm s^2 (the length of the

PHILOSOPHICAL TRANSACTIONS OF THE ROYAL SOCIETY B BIOLOGICAL SCIENCES

wing is 6·04 cm, whereas the length of 6·39 cm employed in the other calculations is the distance from the fulcrum to the indicator point of the wing tip).

In order to counteract the force due to masses at the moment of time under consideration, the thorax must produce a forward-turning torque of $3600 \times 0{\cdot}226 \times 10^{-3} = 0{\cdot}81$ g cm and an upturning one of $-0{\cdot}41$ g cm. In all the thorax must produce a forward-turning torque of $-0{\cdot}17 + 0{\cdot}81 = 0{\cdot}64$ g cm and an upturning torque of $-1{\cdot}80 - 0{\cdot}41 = -2{\cdot}21$ g cm.

At the position considered, the forward-directed angular velocity is $41{\cdot}6\ s^{-1}$ and the upward velocity $-35{\cdot}7\ s^{-1}$. The effect will be

$$0{\cdot}64 \times 41{\cdot}6 + (-2{\cdot}21)\ (-35{\cdot}7) = 106 \text{ g cm s}^{-1}.$$

References

References to other *Parts* of this study are given as part I, part II, etc. The following Parts are printed in this issue:

Part I. Weis-Fogh, T. & Jensen, Martin Basic principles in insect flight. A critical review.
Part II. Weis-Fogh, T. Flight performance of the desert locust (*Schistocerca gregaria*).
Part IV. Weis-Fogh, T. Notes on sensory mechanisms in locust flight.

The following Parts are being prepared:
Part V. Jensen, Martin Strength and elasticity of locust cuticle.
Part VI. Weis-Fogh, T. Wing movements and elastic deformations in flying locusts.
Part VII. Weis-Fogh, T. Functional anatomy of the wing system of the desert locust (*Schistocerca gregaria*), including the tracheal system.
Part VIII. Weis-Fogh, T. Lift and metabolic rate of flying locusts.
Part IX. Jensen, Martin & Weis-Fogh, T. The energetics of locust flight.
Part X. Jensen, Martin & Weis-Fogh, T. General discussion of locust flight.

Abbott, B. C., Bigland, B. & Ritchie, J. M. 1952 The physiological cost of negative work. *J. Physiol.* **117**, 380–390.
Asmussen, E. 1952 Positive and negative muscular work. *Acta physiol. scand.* **28** (1953), 364–382.
Hocking, B. 1953 The intrinsic range and speed of flight of insects. *Trans. R. Ent. Soc. Lond.* **104**, 223–345.
Holst, E. v. & Küchemann, D. 1941 Biologische und aerodynamische Probleme des Tierfluges. *Naturwissenschaften*, **29**, 348–362.
Jensen, Martin 1954 *Shelter effect*. Copenhagen: The Danish Technical Press.
Küssner, H. G. 1936 Zusammenfassender Bericht über den instationären Auftrieb von Flügeln. *Luftfahrtforsch.* **13**, 410–424.
Küssner, H. G. & Schwarz, L. 1940 Der schwingende Flügel mit aerodynamisch ausgeglichenem Ruder. *Luftfahrtforsch.* **17**, 337–354.
Osborne, M. F. M. 1951 Aerodynamics of flapping flight with application to insects. *J. Exp. Biol.* **28**, 221–245.
Rainey, R. C. & Waloff, Z. 1951 Flying locusts and convection currents. *Anti-Locust Bull.* no. 9, pp. 51–70.
Walker, G. T. 1925 The flapping flight of birds. *J. R. Aero. Soc.* **29**, 590–594.
Walker, G. T. 1927 The flapping flight of birds. II. *J. R. Aero. Soc.* **31**, 337–342.
Weis-Fogh, T. 1952 Fat combustion and metabolic rate of flying desert locusts (*Schistocerca gregaria* Forskål) *Phil. Trans.* B, **237**, 1–36.
Wien, W. & Harms, F. [ed.] 1926 *Handbuch der Experimentalphysik*, **1**, Leipzig: Akademische Verlagsgesellschaft.

PHILOSOPHICAL TRANSACTIONS OF THE ROYAL SOCIETY B BIOLOGICAL SCIENCES